TAMPEREEN TEKNILLINEN YLIOPISTO
TAMPERE UNIVERSITY OF TECHNOLOGY

KAISA VUORNOS

DYNAMIC CULTURE OF HUMAN ADIPOSE STEM CELLS IN A FLOW PERFUSION BIOREACTOR

Master's thesis

Examiners: Professor Minna Kellomäki
and Kaarlo Paakinaho, PhD
Supervisor: Docent Suvi Haimi
Examiners and topic approved in the
Engineering Sciences Faculty Council
meeting on 6 April 2016.

TIIVISTELMÄ

TAMPEREEN TEKNILLINEN YLIOPISTO
Materiaalitekniikan koulutusohjelma
VUORNOS, KAISA: Ihmisen rasvakudoksen kantasolujen dynaaminen soluviljely läpivirtausbioreaktorissa
Diplomityö, 75 sivua
Marraskuu 2016
Pääaine: Materiaalitekniikka
Tarkastajat: Professori Minna Kellomäki ja tutkijatohtori Kaarlo Paakinaho
Ohjaaja: Dosentti Suvi Haimi
Avainsanat: kudosteknologia, rasvakudoksen kantasolut, luuerilaistus, dynaaminen soluviljely, läpivirtausbioreaktori

Regeneratiivisen lääketieteen tavoitteena on korjata tai korvata vaurioituneita kudoksia. Kudosteknologiassa yhdistetään kantasoluja biomateriaalien ja liukoisten tekijöiden kanssa, minkä avulla pyritään vastaamaan kudos- ja elinsiirteiden puutteeseen. Luukudosvauriot sekä akuutit traumat yhdessä pidentyneen elinajanodotteen kanssa lisäävät tarvetta tuottaa luuistutteita kudosteknologisesti.

Ihmisen rasvakudoksen kantasolut ovat helposti käytettävissä oleva ja riittoisa lähde monikykyisille hyvin jakaantuville kantasoluille, joita voidaan soveltuvissa *in vitro* olosuhteissa erilaistaa ainakin rasva-, luu-, lihas-, rusto-, ja jännekudoksen suuntaan. Potilaskohtaisten solujen avulla voidaan välttää elimistön hylkimisreaktioita.

Työn tavoitteena oli testata uuden läpivirtausbioreaktorin soveltuvuutta aseptiseen soluviljelyyn. Toisena tavoitteena oli saada aikaan dynaamisen nestevirtauksen avulla ihmisen rasvakudoksen kantasolujen luuerilaistuminen uusissa ylikriittisellä CO_2 -menetelmällä työstetyissä polylaktidi-polykaprolaktonipohjaisissa komposiittitukirakenteissa eli skaffoldeissa, mihin oli sekoitettu 40 % painosta β-trikalsiumfosfaattigranulaa (PLCL-β-TCP).

Biokemiallisina tutkimusmenetelminä sovellettiin alan vakiintuneita analyysimenetelmiä. Läpivirtaussytometrian avulla varmistettiin solujen kantasoluominaisuudet. Solujen elinkykyä tutkittiin kvalitatiivisesti Live/Dead -analyysin avulla ja solumäärä määritettiin kvantitatiivisesti DNA-määrään perustuvalla CyQUANT-analyysilla. Ihmisen rasvakudoksen kantasolujen luuerilaistumista analysoitiin kvantitatiivisesti alkaliinisen fosfataasin (qALP) aktiivisuuden mittauksella, kokonaiskollageenipitoisuuden sekä mineralisaation määrityksellä.

Solut olivat elinkykyisiä kaikissa olosuhteissa. Läpivirtausbioreaktorin avulla saatiin aikaan korkeampi solumäärä sekä virtausnopeus- että rakennevertailussa. Kanavaskaffoldeissa solut olivat jakaantuneet tasaisimmin rakenteeseen. Dynaamisessa olosuhteessa qALP-, kokonaiskollageenipitoisuus- sekä mineralisaatiotulokset olivat samalla tasolla tai alhaisempia kuin staattisessa kontrolliolosuhteessa kaikissa kokeissa. Ihmisen rasvakudoksen kantasolujen luuerilaistumista ei saatu aikaan läpivirtausbioreaktorissa perussoluviljelymediumissa ilman lisättyjä kemiallisia tekijöitä. Tarvittaisiin lisäkokeita, että voitaisiin selvittää toiminnalliset soluviljelyolosuhteet ja nestevirtausparametrit läpivirtausbioreaktorissa ihmisen rasvakudoksen kantasolujen luuerilaistumisen tukemiseksi huokoisissa PLCL-β-TCP -skaffoldeissa. Uusi läpivirtausbioreaktori soveltuu aseptiseen soluviljelyyn, on helppokäyttöinen ja kustannustehokas.

ABSTRACT

TAMPERE UNIVERSITY OF TECHNOLOGY
Master's Degree Programme in Materials Engineering
VUORNOS, KAISA: Dynamic culture of human adipose stem cells in a flow perfusion bioreactor
Master's thesis, 75 pages
November 2016
Major: Materials Engineering
Examiner: Professor Minna Kellomäki and Kaarlo Paakinaho, PhD
Supervisor: Docent Suvi Haimi
Keywords: tissue engineering, adipose stem cells, osteogenic differentiation, dynamic cell culture, flow perfusion bioreactor

Regenerative medicine aims to restore or replace damaged tissue functions. Tissue engineering offers a solution to the growing shortage of suitable tissue and organ donors by combining stem cells with biomaterials and soluble factors. Bone defects and acute traumas together with increased life expectancy augment the demand for new tissue engineered bone tissue constructs.

Among multipotent mesenchymal stem cells, human adipose stem cells (hASCs) are an abundant and accessible source of adult stem cells with capacity to proliferate and differentiate *in vitro* towards at least fat, bone, muscle, cartilage, and tendon tissues under appropriate conditions. With autologous cells, the risk of adverse immunological reactions is reduced.

The aim of this work was to test the suitability of a new flow perfusion bioreactor for aseptic cell culture. The dynamic fluid flow was used to induce osteogenic differentiation of the hASCs in novel supercritical CO_2 processed polymer composite scaffolds of polylactide-co-poly-ε-caprolactone with 40 wt-% β-tricalcium phosphate granules (PLCL-β-TCP).

Biochemical analysis methods well established in the field were used. Flow cytometric cluster of differentiation marker expression analysis was used to verify the stem cell properties of the hASCs. Cell viability and adhesion was qualitatively analyzed with Live/Dead fluorescence staining. Cell number was analyzed using a quantitative assay based on the total amount of DNA in the sample. The hASC osteogenic differentiation was assessed by evaluating quantitative alkaline phosphatase (qALP) activity, total collagen content, and mineralization.

Cells were viable in all the conditions. Higher hASC proliferation was obtained with the perfusion flow bioreactor in both the flow rate and structure comparison experiments and uniform cell distribution was gained for the channel scaffolds under perfusion. In the dynamic condition, the results for the qALP, total collagen content, and mineralization analyses were similar or lower compared to the static control in all the experiments. No osteogenic differentiation of the hASCs was achieved in the flow perfusion bioreactor with basic maintenance cell culture medium without added chemical factors.

Further experiments are needed to define the functional cell culture conditions and fluid flow parameters in the bioreactor to support hASC osteogenic differentiation. The new bioreactor system is suitable for aseptic cell culture, easy to use and cost-effective.

PREFACE

This study was carried out at the Institute of Biosciences and Medical Technology, BioMediTech, a joint institute of life sciences and medical technology of the University of Tampere and the Tampere University of Technology.

I would like to thank the thesis supervisor Docent Suvi Haimi, PhD, for the topic and the Adult Stem Cell Group leader Docent Susanna Miettinen, PhD, for advice as well as for the opportunity to learn about bioreactor cell culture, as well as the entire Adult Stem Cells Group for inspiration. I would like to thank the BioMediTech Adult Stem Cells group for the use of stem cells and laboratory resources, and the Tampere University of Technology Department of Electronics and Engineering for the bioreactor prototype and the biomaterials used in this study. The greatest thanks go to my family for their love, support, and humour throughout my studies, and my friends for sharing wide horizons in the seven seas.

Author's contribution

The author conducted all the experimental laboratory work and all the results' analyses. All the hASC isolations and flow cytometric analyses were performed by the Adult Stem Cells Group's laboratory technologist Anna-Maija Honkala. The bacterial contamination tests for all the bioreactor experiments were conducted by the Regea Cell and Tissue Center Quality Management services.

Tampere, 23 November 2016

Kaisa Vuornos

TABLE OF CONTENTS

ABBREVIATIONS AND TERMS

3D	Three dimensional
ALP	Phosphatase transporting alkaline phosphatase
ASC	Adipose stem cell
β-TCP	beta-Tricalcium phosphate
BaG	Bioactive glass
BMP-2	Bone morphogenetic protein-2
BMSC	Bone marrow stromal stem cell
BSP	Bone sialoprotein
Calcein AM	Calcein acetoxymethyl ester
CaP	Calcium phosphate
CD	Cluster of differentiation marker
COL1	Collagen type I
CT	Computer tomography
DMEM/ F-12	Dulbecco's Modified Eagle Medium/ Ham's Nutrient Mixture F-12
DPBS	Dulbecco's Phosphate Buffered Saline
ECM	Extracellular matrix
ESC	Embryonic stem cell
EthD-1	Ethidium homodimer-1
FACS	Fluorescence activated cell sorter
hASC	Human adipose stem cell
HE stain	Hematoxylin and eosin stain
HLA-DR	Human leukocyte antigen HLA class II
hMSC	Human mesenchymal stem cell
HS	Human serum
ICM	Inner cell mass
iPS	Induced pluripotent stem cell
ISCT	International Society for Cellular Therapy
in vitro	Experiment performed in controlled environment, outside of living organism
in vivo	Experiment performed inside living organism
MM	Maintenance medium
MSC	Mesenchymal stem cell
OM	Osteogenic medium
OC	Osteocalcin
ON	Osteonectin
OPN	Osteopontin
OSX	Osterix
PCL	Polycaprolactone
PET	Poly(ethylene terephthalate)
PFA	Paraformaldehyde
PLA	Polylactide
PLCL	Poly(L-lactic-co-ε-caprolactone)

P(L/D)LA	Poly-L,D-lactide
PLGA	Poly(L,D-lactic-co-glycolic acid)
PLLA	Poly(L-lactide)
P/S	Penicillin/streptomycin
qALP	Quantitative alkaline phosphatase activity
RUNX2	Runt domain-containing transcription factor
SD	Standard deviation

1 INTRODUCTION

Skeletal bone injuries requiring a critical sized bone graft affect roughly 1 million patients each year in the U.S. that combined with more than 6 million bone fractures constitute a growing demand for tissue engineered bone grafts [1; 2]. These muscoloskeletal disorders cause considerable healthcare costs worldwide in relation to serious injuries, increased life expectancy, and diminished quality of life. Biomaterials are needed to treat critical-sized bone defects [3] because patient's own autologous tissue is limited and there is a shortage of suitable allograft bone donors, in addition to which immunogenic responses can cause adverse effects and xenograft bone grafts from animal origin carry the risk of transmitting infectious diseases. [2; 4]

According to the tissue engineering strategy, stem cells are differentiated with the support of the biomaterial scaffold structure and stimulation by growth factors [5]. Tissue engineering aims to maintain, improve or restore lost tissue function [5; 6]. In tissue engineering, it is important to utilize materials science to understand concepts of how cells adhere to biomaterial, material surface chemistry, topography and scaffold structure, and what material properties suit specific tissue engineering applications. What is more, also concepts of cell and molecular biology, developmental biology, chemistry and biochemistry together with immunology, tissue and body anatomy and physiology are all founding concepts in tissue engineering. In addition, adjacent fields of biotechnology such as imaging, bioinformatics, computer modeling, microfluidics and actuator technology offer important tools for tissue engineering development.

Cell seeded scaffolds are cultured *in vitro* to induce extracellular matrix (ECM) synthesis and to allow for sufficient cell mass formation. Both are crucial to ensure neotissue growth when the engineered tissue construct will be implanted back to the patient and the site of injury. [7] For functional tissue engineering scaffolds, both high porosity and pore interconnectedness are desirable features for biodegradable materials in addition to a high surface area for cell adhesion [8]. Synthetic composite scaffolds of polymer and ceramic components that are osteoconductive, which means bone supporting, help meet the demand for new bone tissue engineering applications. In a potential tissue engineered bone graft, the polymer component allows the structure to be moulded while the calcium rich ceramic component drives osteoconductive properties together with the interconnected porous structure that permits ingrowth of bone forming cells and formation of vasculature into healing tissue. [9]

Mesenchymal stem cells (MSC), originating from the embryonic mesoderm layer, are stem cells found in the adult and multipotent in their capacity to form at least bone, cartilage, tendon, muscle, skin, fat, and nerve tissue cells [10]. These adult stem cells have the advantage of autologous tissue transplantation avoiding the risks of graft-versus-host disease, while also avoiding the ethical issues related to the use of embryonic stem cells (ESC). The adult stem cells have lower treatment and production costs than the stem cells produced by the induced stem cell technology. The human adipose stem cells (hASC) are highly potential and an abundant source of the MSCs for tissue engineering applications and compared to the bone marrow stromal stem cells (BMSCs), the hASCs have the advantage of a higher yield of stem cells from a volume of tissue sample, while also the clinical procedure poses a smaller risk to the patient than the harvesting of the bone marrow. [10; 11; 12] While skeletal tissue engineering with biomaterials and multipotent mesenchymal stem cells offers a promising combination for the development of various clinical treatments [13], craniomaxillary reconstruction has already been accomplished with hASCs in clinical applications [14].

In cell culture, prolonged *in vitro* expansion is time consuming and costly and increases the risk of cellular genetic aberrations. In order to produce clinically a relevant size bone graft, an efficient and easily accessible cell source is required. Dynamic cell culture with bioreactor based process has been proposed to induce faster, more efficient and homogeneous cell growth in a three dimensional (3D) supporting biomaterial scaffold structure [7], and perfusion flow cell culture has been reported efficient in 3D culture [15; 16; 17; 18; 19; 20; 21; 22; 23; 24; 25; 26; 27; 28; 29; 30; 31; 32]. The osteogenic potential of the hASCs in flow perfusion has demonstrated in recent of studies [33; 34; 35; 36; 37; 38; 39]. The optimal parameters for hASC osteogenic differentiation in dynamic fluid flow cell culture, such as culture duration, flow rate of liquid, or supporting scaffold structure have not yet been defined. For the scaffold, enhanced human mesenchymal stem cell (hMSC) osteogenesis has been observed with the aid of porous ceramic polymer composite biomaterials [40; 41; 42; 43; 44].

For the maturation of the cell seeded construct, efficient oxygen and nutrient flow together with removal of debris are required, and most often with the added activation provided by mechanical stimulation. In this respect, perfusion bioreactors carry the benefits of improved mass transport compared to the traditional static cell culture environment which is limited by the diffusion of soluble species. The mechanical stimulation provided by the fluid flow increases deposition of ECM components such as fibrous collagen and other proteins. [8]. However, up to the present, there has not been available any easy to use, cost effective, and readily upscalable flow perfusion bioreactor for high-throughput aseptic cell culture purposes.

The aim of this work was, firstly, to test the suitability of the novel flow perfusion bioreactor for aseptic *in vitro* cell culture use. Secondly, the work aimed to analyze the potential of hASCs for bone tissue engineering applications by combining hASCs with

new supercritical CO_2 processed polymer composite scaffolds of poly(L-lactic-co-ε-caprolactone) (PLCL) with 40 wt-% β-tricalcium phosphate (β-TCP) in dynamic culture conditions in the novel flow perfusion bioreactor.

Chapter 2 establishes the theoretical background with stem cells and hASCs in bone tissue engineering and the tissue engineering scaffold requirements for bone tissue engineering applications together with the advantages offered by dynamic cell culture, different bioreactor types and perfusion flow bioreactors. Chapter 3 introduces the materials and methods used in this study, and Chapter 4 presents the results of the bioreactor cell culture experiments. Chapter 5 discusses the different aspects of this work and, finally, Chapter 6 presents the conclusions of this study.

2 THEORETICAL BACKGROUND

2.1 Stem cells and bone tissue engineering

Stem cells have emerged as a promising alternative to restore or replace damaged tissues. Bone tissue engineering has developed over past decades to offer real alternatives for critical sized bone grafts.

2.1.1 Stem cells

Stem cells can be embryonic, somatic or of germline origin with extensive capacity to self-renew in long-term culture together with the potential to differentiate into cells of several different tissue types [45; 46]. The differentiation process includes asymmetric cell divisions where one daughter cell differentiates and the other one maintains its stem cell characteristics. [45]

Stem cells possess distinct differentiation potentials. The zygote, or the fertilized egg, is totipotent with the capacity to produce all the cell types of the organism and to replicate indefinitely. The following stage of cellular development, the blastocyst, is composed of undifferentiated inner cell mass (ICM), as well as an outer trophoblast layer. The ICM cells are pluripotent with the capacity to form all embryonic cell types and an indefinite capacity to divide. Generally, it is the ICM that is used as a source of ESCs in research [45]. The somatic stem cells are either adult stem cells or induced pluripotent stem (iPS) cells. The iPS cells are produced in laboratory with somatic cell nuclear transfer or overexpression of pluripotency factors from somatic cells, for example, dermal fibroblasts [47]. However, the reprogramming using viral vectors may cause imbalanced results in cell behavior resulting in teratomas and a large selection of iPS cell lines from multiple sources is needed for balanced results [48].

2.1.2 Mesenchymal stem cells

Most adult tissues have a population of undifferentiated progenitor cells. Whereas ESCs and iPS cells have excellent proliferation and differentiation capacity, the somatic adult tissue stem cells possess limited capacity to divide or to differentiate based on their ectodermal, mesodermal or endodermal embryonic germ layer origin [45]. Despite their limitations, the MSCs are a more readily available cell source and the use of MSCs involves a lower risk of tumorigenicity and helps to avoid the ethical and legal issues related to the use of the ESCs. Also, the use of a patient's own autologous cells bears no risk of immunogenic reactions [10; 45; 46].

Ectodermal tissues encompass neural, dermal and ocular tissues, whereas mesodermal tissues include the bone marrow, adipose, cardiac, bone, cartilage and muscle tissues of

the body. Finally, endodermal tissues comprise pulmonary, hepatic, pancreatic and ovarian tissues or testicular stem cells [45]. The bone marrow, for example, is mesoderm derived tissue that harbors the hematopoietic stem cells producing mature blood cells in addition to the MSCs, the non-hematopoietic stromal cells. According to the International Society for Cellular Therapy (ISCT) minimal criteria, the MSCs are plastic-adherent in standard cell culture conditions and ≥95 % of the cell population should express specific surface antigens or cluster of differentiation markers (CD), namely CD73, CD90, and CD105 and <2 % express CD11b, CD14, CD19, CD34, CD45, CD79a and human leukocyte antigen HLA class II (HLA-DR) [49]. In addition, they must have ability to differentiate towards bone, adipose and cartilage tissues [49]. More specifically within different types of MSCs, ASCs express CD36 and lack the expression of CD106 as opposed to BMSCs [50].

2.1.3 Adipose stem cells

The hASCs were first characterized by Zuk and coworkers (2001) [51] as MSCs with multilineage differentiation capacity to differentiate into at least osteogenic, adipogenic and chondrogenic lineages, according to the definition of the MSCs [49]. The adipose stem cells (ASCs) are characteristically plastic adherent and have a certain cell surface marker expression pattern to aid characterize the stem cells [51]. Since then, differentiation of the hASCs also towards nerve, tendon, and muscle tissues has been published [52; 53]. The subcutaneous adipose tissue comprises besides adipocytes and hASCs, also a heterogeneous supportive cell population, all of which combined form the stromal vascular fraction. The hASCs have the advantage of abundance and availability over other types of adult stem cells. The yield percentage of hASC isolation from subcutaneous adipose tissue is considerably higher when compared to hBMSCs, for example. In addition, the clinical harvesting procedure poses a smaller risk to the donor patient than the harvesting of the bone marrow for hBMSC isolation. _ Figure 1 shows the phenotypical spindle-shaped hASC morphology.

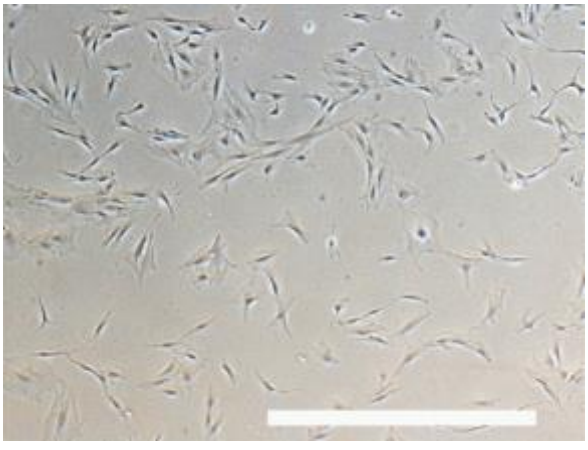

***Figure 1**. Human adipose stem cells (hASCs). Brightfield image on polystyrene cell culture plastic (Anna-Maija Honkala, 2012). Magnification ×10, scale bar 1 mm.*

The hASCs are well-suited for *in vitro* expansion. [10]. Because hASCs proliferate rapidly in culture, populations can readily reach the large cell numbers needed for clinical applications. The ease of harvest, large number of cells, and rapid in vitro expansion are notable advantages of hASCs over hBMSCs [54]. Furthermore, the hASCs are genetically more stable than the hBMSCs in long-term culture [55], which makes them an attractive choice for cellular applications. The adult tissue stem cells have the advantage of autologous tissue transplantation avoiding the risks of graft-versus-host disease. The use of autologous undifferentiated stem cells also helps to avoid immune rejection, which is a major advantage when considering clinical applications. [10]

The hASCs have already been used in clinical applications for critical size bone grafts. Several patients suffering from craniomaxillary injuries have already been treated with autologous hASCs in combination with calcium phosphate (CaP) based biomaterials [14; 54; 56].

2.1.4 Bone tissue

Bone tissue consists of hydroxyapatite $Ca_{10}(PO_4)_6OH_2$ mineral phase along with elastic collagen fibers and cells. Hydroxyapatite is able to withstand compression loads but risks breaking under large shear or tensile loads as a hard and brittle material. On the contrary, collagen fibres can easily take on tensile loading but have poor performance in compression. [57] Typically, bone tissue has tensile strength of 120–150 MPa, modulus of elasticity of 17–20 GPa, and compressive strength of 100–160 MPa. Bone tissue has two distinct forms, namely compact and cancellous bone, which have different structures in macroscale; compact bone forms a dense and solid tissue, typically located on the thick outer layer of the shaft of long bones, whereas cancellous bone forms a network of bone spicules which form the ends of long bones, covered by a thin layer of compact bone. [58]

In the microscale, parallel to the long axis of bone, there are irregular cylindrical osteons that have central canals (Figure 2). Around the central canal there is concentric bone tissue lamellae that form the Haversian systems that are connected laterally towards bone surface via the Volkmann's canals. In the bony lamellae, there are small lacunae pores where osteocytes are located. The osteocyte containing lacunae are connected by narrow interconnected channels.

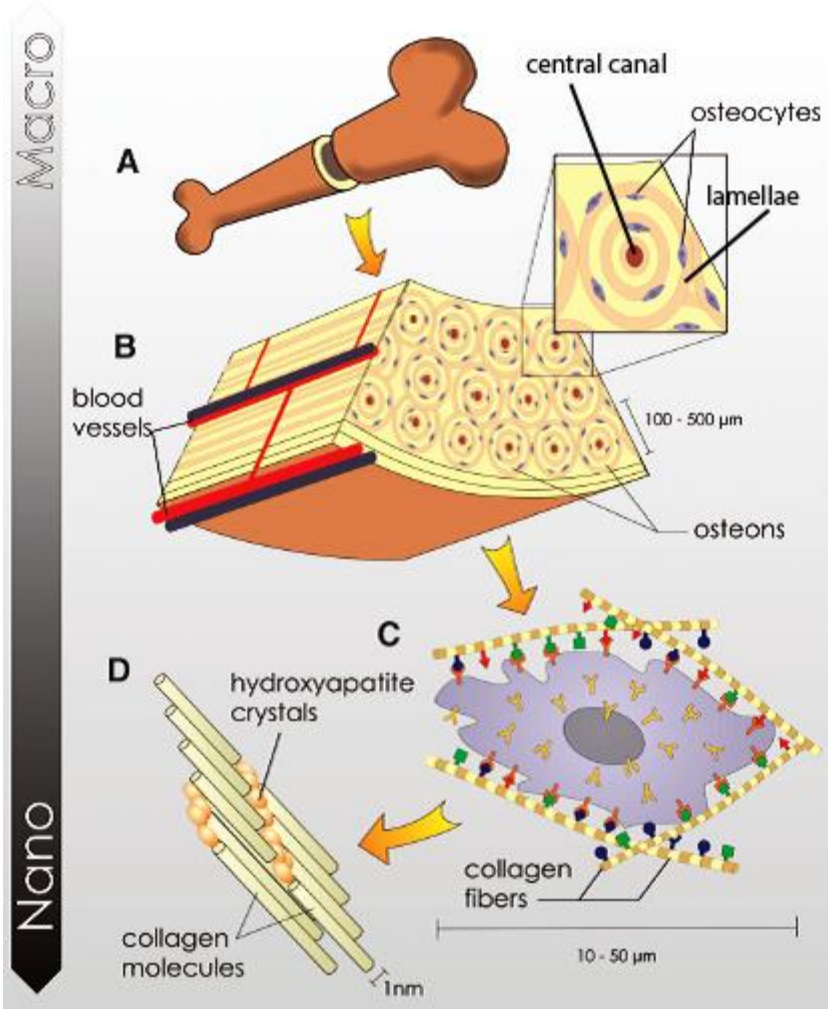

***Figure 2**. Bone tissue organization. A) Compact bone outer layer; B) Osteons with lamellae structure, central canal and osteocytes; C) Bone cell membrane surface receptors with specific binding sites for bone matrix components including fibrous collagen; D) Bone matrix organization with collagen fibers and hydroxyapatite crystals. Modified from [59].*

Bone tissue functionality relies on lacunocanalicular fluid flow which transports oxygen and soluble nutrients and allows removal of osteocyte waste products. Bone lacunocanalicular fluid flow also provides biomechanical stimulation for the cells and induces mechanotransduction processes. [60; 61; 62] Physiological load induced fluid flow shear stress in bone tissue, estimated at 5 kPa [63], supports bone cell maturation and solidifies bone tissue. However, the more precise physiological fluid flow induced biomechanical cues or structural features involved remain to be detailed [63; 64].

2.1.5 Osteogenic differentiation

Osteogenic differentiation of hASCs proceeds via activation of biochemical cues in sequential phases of initiation and commitment towards matured cells (Table 1). The hASCs develop towards bone-like cells by cell growth, gene expression of osteogenic marker genes which inititate protein expression of bone ECM components, which consists mainly of fibrous collagen. Bone tissue development progresses with mineralization of

collagenous ECM when CaP residues accumulate, form mineralization nodules and condense into hydroxyapatite, the main structural component of mineralized bone tissue. [58; 65; 66]

Table 1. *Osteogenic marker genes in hASC osteogenesis process [67].*

Commitment	**Maturation**	**Mineralization**
RUNX2	OSX	OC
DLX5	COL1	DLX5
ALP	ALP	OPN
		BSP

Maturation to bone can proceed either via intramembraneous ossification where MSCs condense and differentiate into bone forming cells, or by endochondral ossification where MSCs differentiate into chondrogenic cell type before maturing into bone osteoblasts to form bone ECM [67]. Cell differentiation and tissue maturation processes proceed with the aid of molecular switches involved in cell signaling routes including a number of transcription factors, growth factors, cytokines, cell signaling molecules, and cell receptors [68].

Osteogenic gene expression markers that are activated early in the differentiation process include RUNX2, a runt domain-containing transcription factor, which operates upstream from zinc finger protein osterix (OSX). [65; 67; 69; 70] A transcription factor DLX5 and phosphatase transporting alkaline phosphatase (ALP) protein are also involved in early osteogenic differentiation. Late markers of hASC osteogenic differentiation differentiation include bone ECM proteins such as collagen type I (COL1), ALP protein, osteopontin (OPN), osteonectin (ON), bone sialoprotein (BSP) and osteocalcin (OC). [71]. Accumulation of collagenous matrix indicates hASC osteogenic differentiation, whereas the accumulation of calcium phosphatase enzyme is signaled by the activity of the phosphatase transporting ALP protein on cell membrane before matrix mineralization. Calcium binding ECM proteins, such as OPN, help mineralize the bone matrix by forming mineral crystals such as hydroxyapatite [70]. Bone matrix CaP complexes which in turn form hydroxyapatite can be analyzed by calcium binding staining such as Alizarin Red S stain. The fibrillary collagen network of bone ECM is mineralized via calcium binding.

Osteogenic differentiation of hASCs needs to be verified by analysis of osteogenic markers of gene and protein expression, cell morphology and also by *in vivo* tissue sample histology. Despite the known biochemical processes of bone ECM formation, it is important to bear in mind that the degree of differentiation varies in a stem cell population and this might cause variation in results of *in vitro* analyses in addition to donor dependent variation. [69]

For *in vitro* experiments, stem cell commitment towards osteogenic lineage has been enhanced by various stimuli, including chemical induction by differentiation medium

optimized for hASCs containing ascorbate-2-phosphate, β-glycerophosphate and dexamethasone [72]. However, the usability of growth factors is limited because of superphysiological concentrations required for *in vitro* culture and the related high costs, in addition to risks involved in the use of exogenously produced chemical supplements which are undesirable considering possible clinical treatments [73; 74; 75]. Their effect might also be questioned since exogenously added growth factors might not after all enhance hASC osteogenic differentiation [72]. Electrical stimulation [76], vibration loading [77] and surface topographic cues as mechanical stimulation [78; 79] have also been applied for osteogenic induction of hASCs. Indeed, the need for added soluble factors could be surpassed by mechanical stimulation, for example. The mechanical stimulus in the mechanotransduction process activates chemical and electrical signals inside the cell, although also osteoblast mechanosensitivity remains largely undetermined. [62; 80; 81].

The scaffold architecture, cell density, and pore size are also important factors for hASC osteogenic differentiation [72]. Previously, a pore size of 200–600 μm has been used to induce hASC osteogenesis [82] [p. 409].

2.2 Scaffolds for bone tissue engineering

Tissue engineering scaffolds are structures that support the growing cells and regenerating tissue at the site of injury. There are a number of important requirements that need to be met to assure good cell-material interactions. Composite biomaterials allow to combine the desired properties of different materials and can be designed for specific applications. A biomaterial that supports bone cell growth is in literature termed osteoconductive, a bone inducing biomaterial is referred to as osteoinductive and an osteogenic biomaterial triggers bone formation. Certain biomaterials, for example PLCL and CaP, are especially well suited for bone tissue engineering applications [83; 84]. Besides the choice of material, the structure can add important features to the scaffold and, for example, a highly porous irregular structure can be fabricated with a supercritical CO_2 method [85].

2.2.1 Tissue engineering scaffold requirements

The scaffold requirements are tissue specific and depend on the site and severity of the injury. Tissue engineering scaffolds provide structural support and function as load bearing structures for healing tissue. Mechanically, the scaffold should have properties with suitable strength, stiffness, Young's modulus, toughness, durability and elasticity. The scaffold material and architecture should also maintain sufficient mechanical properties before tissue regeneration and scaffold biodegradation and resorption. [57] In addition, similar scaffold degradation and tissue formation rates would ensure functionality of load bearing grafts in bone applications. A biodegradable structure that supports cell adhesion, proliferation, ECM deposition and *in vivo* ingrowth of bone

forming cells is preferred [86]. Biodegradable material disappears with tissue regeneration, thus avoiding need for second surgery to remove implant. A bioresorbable scaffold that degrades into natural metabolism end products reduces risk of harmful pH alterations or tissue infection at the implantation site [87]. A highly porous structure possesses also less bulk material to be processed by tissue metabolism [88]. Biomaterial biocompatibility is an important scaffold requirement to support cell growth without inducing cytotoxic, disadvantageous inflammation or adverse immune reaction [89].

Cell culture in a 3D scaffold provides the cells with a topographic microenvironment more similar to native tissue [90]. The cues from the correct microenvironment guide stem cells to differentiate and also help differentiated cells to maintain their phenotype [91]. The physical scaffold properties include pore size, pore orientation, and their interconnectedness contribute to the scaffold function and to the creation of cell microenvironment. The scaffold interior architecture should allow cell growth through the structure to ensure homogeneous cell distribution and implant quality. To gain sufficient cell density for tissue regeneration interior the construct, high scaffold porosity with a high surface to volume ratio provides growing cells with interactions with biomaterial surface and an adhesion surface. Therefore, high porosity and an interconnected pore network are important scaffold requirements in the limits of scaffold mechanical strength. [57] An interconnected porous network facilitates transport of gas, nutrient and metabolic waste products throughout the structure thus maintaining cell viability and proliferation. Also, in the case of vascularized tissues such as living bone tissue, selected biomaterial should support angiogenesis of vascularized tissues and also structural space must be provided in the scaffold for the formation of vasculature to maintain the viability of the developing 3D cellular network. [57; 92] Therefore, open and accessible porosity throughout the construct are needed for fluid inflow and bone ingrowth into the construct [58] [p. 16]. The interior scaffold architecture should mimic natural cell microenvironment to support cell functionality. Tissue specific mechanical properties are also important scaffold requirements directing cell fate and to support tissue load bearing. [93; 94]

Scaffold materials utilized for tissue engineering range from decellularized tissue matrixes to synthetic and natural biomaterials. Whereas decellularized tissue matrixes similarly depend on availability of suitable donors, and while natural biomaterials might elicit unwanted immunological side effects or chronic inflammation, or have less predictable rate or mechanism of degradation, poor mechanical properties or might suffer from patch to patch variation or harmful viral antigens, synthetic biomaterials offer an attractive alternative with controlled quality. Synthetic polymers are widely applied biomaterials in tissue engineering applications [95] due to their tissue compatibility and because they are immunologically inert. It is possible to achieve a tailored degradation rate with synthetic polymers and maintain sufficient mechanical properties while native tissue has healed [96]. In addition, the synthetic polymer material production process is repeatable and allows for large scale production [97]. However, they lack adhesion sites

of bioactive molecules to facilitate cell adhesion and growth on biomaterial surface. Therefore, synthetic biomaterials might benefit from functionalization. Composite scaffolds might also include an inducing factor, such as an osteoconducting or osteoinducing component, to direct or regulate tissue growth to induce formation of new tissue. [98; 99] The scaffold design should be suitable for target tissue, for example, chronOS bone graft is a synthetic β-TCP granule based bone void filler with sodium hyaluronate powder which is osteoconductive, bioresorbable, and flexible for remodeling at site of injury (Figure 3) [100; 101].

Figure 3. *Commercial chronOS bone graft substitute fabricated by DePuy Synthes* [102].

Suitable surface chemistry and surface topography for favorable cell-material interactions that support stem cell differentiation are also important scaffold requirements. Scaffold surface topography and material stiffness also provide mechanical cues for the cells. [103]

2.2.2 Polylactide-co-poly-ε-caprolactone and β-tricalcium phosphate scaffolds for bone tissue engineering

Polylactide

As a polymer of lactic acid, polylactide (PLA) is readily biocompatible and bioabsorbable [104]. PLA is an aliphatic polyester and has been used widely in various tissue engineering applications [105], including bone and musculoskeletal tissue engineering [106; 107; 108]. Pure homopolymer poly(L-lactide) (PLLA) is a hard, brittle and semicrystalline polymer (Figure 4) [105].

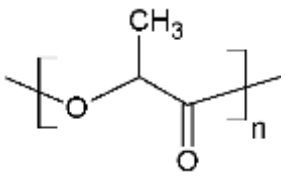

Figure 4. *Molecular structure of poly(L-lactide) (PLLA).*

PLLA is degraded hydrolytically in approximately 2 years in the body into L-lactic acid, a naturally occurring metabolite that is eventually metabolized in the citric acid cycle into water and CO_2. The addition of D-lactide yields a copolymer of lower stiffness and faster hydrolytic degradation rate. This allows tailoring of copolymer mechanical properties and degradation rate. [109] What is more, PLA is not bioactive and requires active components for bone regeneration [105; 110].

Poly-ε-caprolactone

Poly-ε-caprolactone (PCL) (Figure 5) is an aliphatic biodegradable polyester like PLA, highly elastic, and hydrophobic polymer [111]. Due to its semi-crystalline structure and hydrophobicity, PCL degrades in 2–3 years in the body by surface degradation [112; 113]. PCL has been shown to support osteoblastic cells under perfusion flow [32], and has been applied to bone regeneration in perfusion bioreactor culture [114]. In a previously published study, PLCL has been shown to support ASC adhesion and osteogenic differentiation [84].

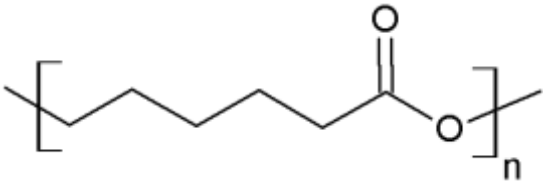

Figure 5. *Molecular structure of polycaprolactone (PCL).*

The addition of PCL ameliorates the elastic properties of L-lactide in the PLCL copolymer structure [113]. PLCL is highly elastic and cytocompatible with hASCs [53; 115; 116]. However, PLCL has been reported to cause formation of fibrous tissue, indicating surface interaction issues and might benefit from surface functionalization [84].

Bioceramics

Porous ceramic biomaterials have been widely used to induce bone regeneration [117; 118; 119]. The synthetic bone substitutes have mainly been based on hydroxyapatite, coralline hydroxyapatite, TCP, biphasic CaP and various types of bioactive glass (BaG) [120]. Bioceramics are osteoconductive materials that support cell adhesion, growth, differentiation, and migration. They are hard and brittle materials and therefore challenging to process. The properties hydroxyapatite, CaP as well as sulphates, are well suited for bone grafts due to their similarities with native bone tissue [84]. In contrast, degradable biopolymers are readily tailorable but not osteoconductive and hydrophobic, such as PLCL. The ceramic biopolymer composites offer an opportunity to combine the osteoconductive and more elastic properties. Mechanical strength of composites is lower than that of bioceramics, while the addition of a ceramic component enhances the mechanical properties of the structure and the polymer allows more elastic properties to

the composite material [121]. An osteoconductive material, such as β-TCP, also promotes bone matrix deposition and offers mechanical support while the biodegradable scaffold is replaced by newly forming tissue. As an added feature, CaP buffers acidic degradation products of PLA [122]. It degrades faster compared to hydroxyapatite and therefore is a suitable choice for bone constructs [122; 123]. Moreover, β-TCP has been shown to promote cell adhesion, proliferation, and osteogenic differentiation of MSCs and healing of bone defects [41; 124; 125; 126]. However, in another study, soluble β-TCP failed to promote osteoblastic cell adhesion and spreading due to high phosphate and low calcium levels in the cell-material interface [127].

Poly(lactide-*co*-ε-caprolactone)-β-tricalcium phosphate

Medical grade poly-L-D-lactide (P(L/D)LA) 96/4 copolymer with sufficient elasticity and mechanical strength was selected for engineered bone construct biomaterial to fabricate biodegradable polymer composite scaffolds of PLCL (Figure 6) with 40 wt-% β-TCP $Ca_3(PO_4)_2$ as an osteoconductive ceramic component. The PLCL-β-TCP composite scaffolds were fabricated with a supercritical CO_2 method with the aim of interconnected porous structure and homogeneous porosity [111].

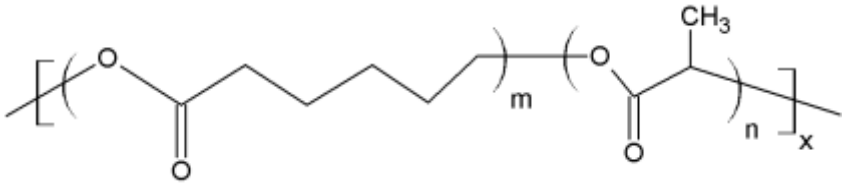

Figure 6. *Molecular structure of poly(L-lactic-co-ε-caprolactone) (PLCL) polymer.*

2.2.3 Supercritical carbon dioxide polymer processing

CO_2 is a noncytotoxic solvent and permits solvent free production of porous materials through generation of gas bubbles within a polymer where it functions as a pore generating agent or a porogen. Supercritical CO_2 processing method is based on the concept that CO_2 is a fluid above its critical temperature of 304.25 K and pressure of 72.9 atm or 7.39 MPa [85]. Above critical temperature and pressure limits, supercritical CO_2 has properties of a gas and fluid as a supercritical fluid, when it expands and fills the container as a gas and but with the density of a liquid. In the melt extrusion fabrication process moulded polymers can be pressurized with CO_2 until polymer is saturated after which the release of pressure results in nucleation and growth of air bubbles (Figure 7). The low production temperatures would also allow the incorporation of temperature sensitive drugs or growth factors as tissue growth supporting soluble species into the processed biomaterial. [9; 85; 128; 129]

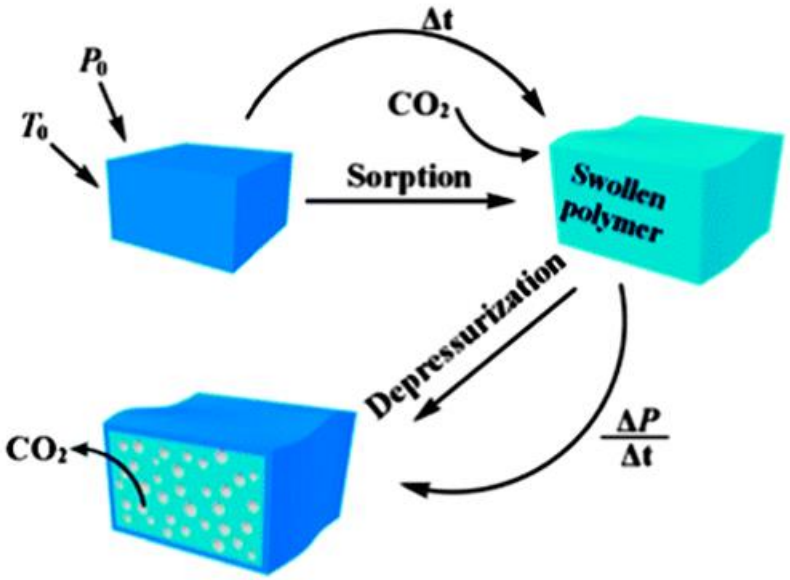

Figure 7. *Supercritical CO_2 processing of polymers. Modified from [129].*

2.3 Dynamic cell culture

Traditionally, static culture has been the standard protocol for *in vitro* cell culture. Generally, the cells are seeded passively by pipetting manually the cell suspension onto the surface of scaffolds [130], after which the cells are allowed to spread gradually towards the scaffold interior under static culture conditions. However, this might lead to limited cell ingrowth, especially in case of a porous structure because cells grow mainly on the exterior surface forming a dense layer that prevents diffusion and transport of nutrients or gas inside to scaffold interior [20]. The cells are also prone to grow on the scaffold periphery where there are more nutrients available from surrounding cell culture medium. This typically results into cell necrosis in the center of the scaffold, and eventually, nonhomogeneous tissue growth and immature tissue construct. On the other hand, dynamic cell culture promotes faster and more homogeneous cell ingrowth and ECM production [131] which augments the stiffness and mechanical properties of the construct [132].

The range of passive diffusion limiting size of tissue engineered constructs varies according to estimates between 240 μm and 3 mm [60; 133]. Dynamic cell culture, for example in a perfusion flow bioreactor, improves survival of critical size tissue engineering constructs with dimensions in millimeter scale. [57; 134; 135] In comparison, in static *in vitro* culture, osteoblastic cells have been reported to form mineralized matrix only to the depth of 240 μm on poly(L,D-lactic-co-glycolic acid) (PLGA) scaffolds.

Typically, the static method requires longer cell culture periods which increases the microbial contamination risk associated with additional handling steps [136]. In tissue engineering production protocols, the effect of the person conducting the manual work

has been exceedingly large. Worker dependent process variability lowers the process repeatability and consistency leading to irregular quality. [57; 130] Dynamic culture has been shown to stimulate stem cell differentiation [114; 137; 138] and also to induce hASC differentiation by mechanical stress [77].

2.3.1 Bioreactor types for bone tissue engineering

Bioreactors as 3D culture systems have been used to control and monitor cues to stimulate growing and differentiating stem cells towards specific lineage [127]. Different types of bioreactors have been tested for bone tissue engineering applications [137]. In a spinner flask (Figure 8A), the cell seeded constructs are pinned to long needles attached to the flask cap and immersed in the culture medium. At the bottom of the flask, a magnetic stirrer mixes the medium constantly [23]. However, the spinner flask is not enough to encourage cell penetration deeper into porous constructs and fluid flow shear stress is concentrated on the cell seeded scaffold surface. A rotating wall bioreactor (Figure 8B) consists of two concentric cylinders of which the outer one rotates whereas the inner one is stationary and permeable to gas diffusion. The constructs are placed inside the cylinder space and maintained in a microgravity-like state by the action of the rotating outer layer while stimulated by hydrostatic pressure. [139; 140]

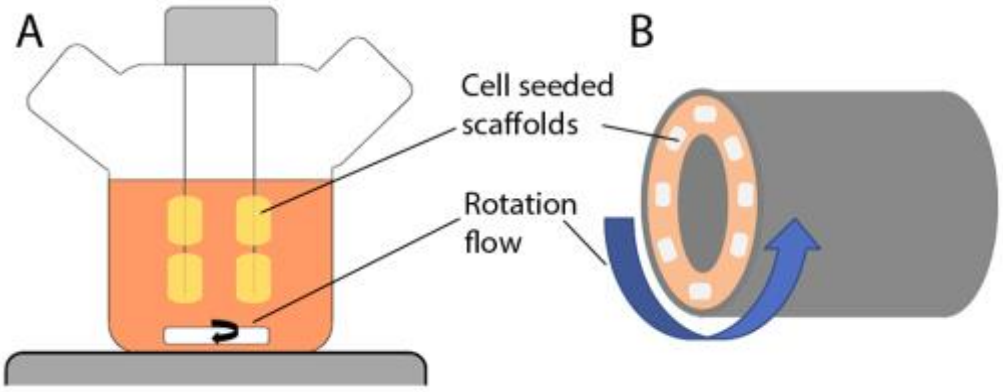

Figure 8. *Bioreactor designs. A) Spinner flask; B) Rotating wall bioreactor. Modified from [137].*

In a rotating wall bioreactor, the shear forces are more moderate than in a spinner flask, but the constructs bounce against each other randomly and the direction of the fluid flow is not controlled [141]. In a flow perfusion bioreactor, the circulating fluid is pumped straight through porous construct for efficient mass transport and mechanical stimulation by fluid shear stress. With different flow rates and depending on the porous structure, it is possible to adjust the fluid shear stress to stimulate cells. [23] For example, under perfusion flow, rat BMSCs were more evenly distributed into porous polymer scaffold and showed higher ALP activity, when compared to spinner flask or rotating wall bioreactors [142].

2.3.2 Perfusion flow bioreactors

A perfusion bioreactor consists of a pump system with tubing that perfuses media through tissue engineering constructs thus providing growing cells with mechanical stimulation. The system is composed of a pump, a culture media reservoir, a tubing circuit and a reactor chamber to hold the porous scaffolds (Figure 9). [136]

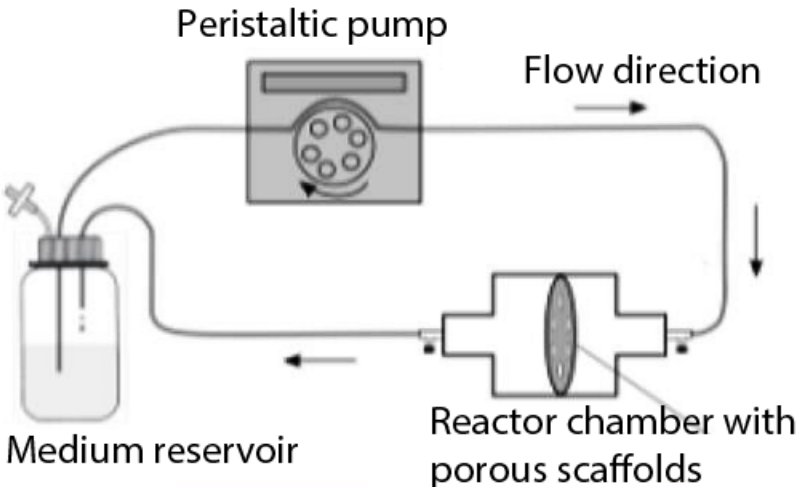

Figure 9. *Schematic presentation of a flow perfusion bioreactor. A culture circuit with constant unidirectional flow by a peristaltic pump through porous scaffolds in a reactor chamber and a medium reservoir. Modified from [143].*

Perfusion flow bioreactors enhance mass transport to the entire 3D scaffold volume by perfusing fluid directly through the constructs to overcome the limitations of diffusion distance. In addition to minimizing diffusional distances, perfusion exposes the cultured cells to controllable hydrodynamic shear forces which can be tailored to direct cell behavior. [133; 144; 145] Perfusion flow systems have been demonstrated to effectively promote homogeneous cell distribution in the scaffold volume, upregulate osteogenic markers, and enhance mineralization [23; 26; 29; 30; 136; 137; 146; 147]. The fluid shear stress has increased production of ALP that is an early bone regeneration marker together with mature bone ECM components such as COL1 along with mineralization of cellular matrix [136; 148]. Higher ALP and cell distribution gained under perfusion compared to spinner flask and rotating wall bioreactor culture in PLGA scaffolds [142].

It has been known that fluid flow stimulates bone cells and secretion of bone markers [149; 150; 151; 152; 153; 154; 155]. Moreover, the dynamic fluid flow has been shown to enhance osteogenic differentiation of hMSCs [156], and ASCs [33; 34; 36]. In a study by Rodrigues et al. (2012) flow perfusion bioreactor was shown to enhance hASC proliferation, homogeneous distribution and osteogenic differentiation in silanol functionalized corn starch PLCL 30/70 scaffolds under perfusion flow [35]. Some relevant perfusion bioreactor *in vitro* studies are listed in Table 2 for comparison.

Table 2. *Perfusion flow bioreactors in cell culture studies for osteogenic differentiation.*

Perfusion flow	**Flow rate [mL/min/ scaffold]**	**Cells**	**Scaffold**	**Medium**	**Time**	**Results**	**Reference**
continuous or pulsatile	steady 0.3, pulsatile 0.3-0.9	hASCs	silk fibroin	OM	5 weeks	OPN+; proteins: COL1+, OPN+, OC+, BSP+, mineralization with 2 weeks of steady flow + 3 weeks of pulsatile flow (2 h pulse flow + 10 h steady flow)	[34]
continuous	0.1	hASCs	BaG foam	MM, OM	21 d	proliferation+, ALP+, OPN+, OC+. Weak hASCs differentiation without chemical stimulus	[33]
continuous	0.1	hASCs	starch-PLCL-Si	MM, OM	21 d	MM, OM: hASCs spread under perfusion, ALP+; OM only: mineralization+	[35]
continuous	0.3	hASCs	decellular bone	MM, OM	5 weeks	OM only: BSP+, OPN+, COL1+	[157]
continuous + compression	0.3, 0.5, 2.0	hASCs	PLGA-CaP	MM	2 weeks static + 9 d perfusion + compression	all: OP+, 2.0 rate: distribution+	[158]
pulsatile	1.0	hBMSCs, hASCs	hydroxyapatite	OM	5 d	efficient *in vivo* engraftment	[159]
pulsatile	3.0	hASCs	hydroxyapatite	MM	5 d *in vitro* + 8 weeks *in vivo*	*in vivo*: HE staining+, BSP+	[160]
continuous	0.1	hBMSCs	silicate-TCP	MM	21 d	ALP+, OPN+, RUNX2+, BSP+, BMP2+	[15]

Perfusion flow	Flow rate [mL/min/ scaffold]	Cells	Scaffold	Medium	Time	Results	Reference
continuous	0.1	hBMSCs	porous PET	MM	40 d	14 d: proliferation-, ALP+, mineralization+, 40 d: ON+	[18]
continuous: parallel or traverse	0.2	hBMSCs	porous PET	MM, OM	14 d	7d MM parallel flow + 7d OM traverse flow: proteins: COL1+, OC+	[19]
continuous	3.0, 6.0, 9.0	hBMSCs	β-TCP	OM	28 d	0.015 Pa fluid flow shear stress and 3 mL/min flow rate: ALP activity+; proteins: OPN+, OC+. Level of shear stress determined results.	[161]
continuous: parallel	0.1, 1.5	hBMSCs	porous PET	MM	20 d	0.1 ml/min: proliferation+; 1.5 ml/min: osteogenic differentiation+	[162]
continuous	0.2	hBMSCs	PLGA	MM, OM	14 d	MM, OM: proliferation+, OM only: ALP+, OPN+, mineralization+	[21]
pulsatile	0.8	hBMSCs	PLCL	MM	7 d	4x 5 min pulse/h: RUNX2+, OPN precursor+, COL1+, mineralization+	[163]
continuous	0.05, 0.17, 0.50	rat BMSC	Ti mesh	OM	16 d	0.05 rate: ALP+ (8 d), OP+ (13 d); 0.17 rate (16 d): proliferation+, ALP+, mineralization+, HE histo+	[164]
continuous	1.0	rat BMSC	electrospun PCL	OM	16 d	ALP+, mineralization+, bone ECM proteins: MMP-2+, PEDF+, COL1+	[165]

Perfusion flow	Flow rate [mL/min/ scaffold]	Cells	Scaffold	Medium	Time	Results	Reference
continuous	0.3	rat BMSC	starch-PLCL	OM	15 d	cell distribution+, mineralization+, ALP-	[25]
continuous	1.0	rat BMSC	starch-PLCL	OM	15 d	scaffold porosity 75 %: proliferation+, ALP+, mineralization+	[26]
continuous	1.0	rat BMSC	Ti mesh	MM, OM	16 d	OM only: ALP+, OPN+, mineralization+	[27]
continuous	1.0	rat BMSC	hydroxyapatite-β-TCP	OM	16 d	proliferation+, ALP+	[145]
continuous	0.6	rat BMSC	fibrous PLLA	OM	16 d	distribution+, ALP+, mineralization+	[29]
continuous	0.3	rat BMSC	Ti mesh	OM	16 d	shear stress (in 6 % dextran) increase instead of flow rate for mineralization+	[30]
pulsatile	0.008	mouse pre-osteoblasts	PCL	OM	28 d	ALP+	[166]

Effects of perfusion flow bioreactor compared to static control: (+), positive effect; (=), no effect; (-), negative effect. Results are reported for gene expression and protein expression results are duly indicated. ***Abbreviations:*** *ALP, alkaline phosphatase activity; BaG, bioactive glass; BMP2, bone morphogenetic protein-2; BSP, bone sialoprotein; COL1, collagen type I; hASCs, human adipose stem cells; hBMSCs, human bone marrow stem cells; HE stain, hematoxylin and eosin stain; MM, maintenance medium; OC, osteocalcin; OM, osteogenic medium; ON, osteonectin; OPN, osteopontin; PCL, polycaprolactone; PET, poly(ethylene terephthalate); PLGA, poly(lactic-co-glycolic acid); PLCL, poly(L-lactic-co-ε-caprolactone); TCP, tricalcium phosphate.*

Several perfusion bioreactor systems have been developed and tested for bone tissue engineering purposes [23; 159; 167; 168]. TA Instruments is a commercial supplier that offers a multispecimen flow perfusion bioreactor system for cell culture with a basically adaptable and scalable setup (Figure 10).

Figure 10. *TA Instruments 3D CulturePro Bioreactor system for multiple single samples [169].*

EBERS Medical has an alternative commercial perfusion bioreactor available. The EBERS multiple sample system has individual chambers for cylindrical scaffolds to direct perfusion flow through the whole scaffold volume (Figure 11A;B).

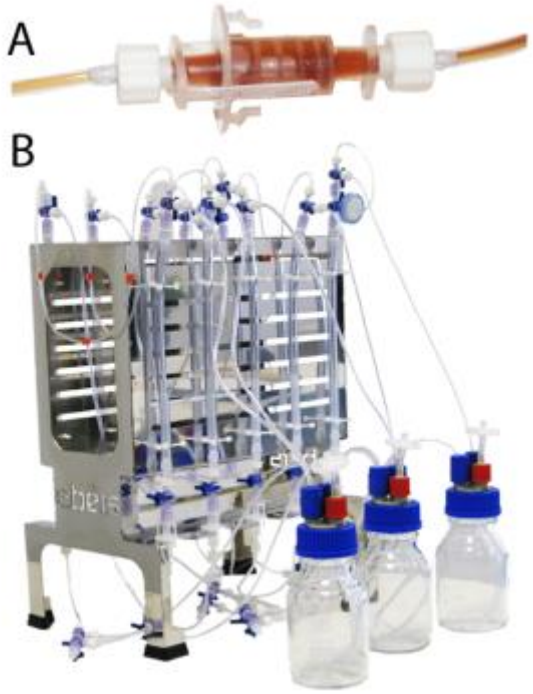

Figure 11. *EBERS Medical P3D flow perfusion bioreactor system A) Individual chamber; B) Multichamber assembly [170].*

In this study, a custom made flow perfusion bioreactor prototype with reusable and easily maintained parts was tested for *in vitro* cell culture use. The bioreactor assembly is presented in more detail in Chapter 3.2 and its functionality is assessed in Chapter 5.5.

The intrinsic fluid flow in bone tissue provides developing cells with mechanical stimulation which is also involved in activating the cell signaling routes. Perfusion flow provides mechanical stimulation for cells in the form of fluid shear stress. [81] This physical stimulation modifies cell response by mechanotransduction process, where mechanical signals are converted into biochemical or electrical signals transmitted via focal adhesions leading to changes in the cytoskeleton (Figure 12) [171].

Figure 12. *Cell response to fluid flow shear forces. Modified from [134].*

The parameters of dynamic fluid flow influencing cells include fluid viscosity and shear stress, in addition to flow parameters such as flow rate and flow direction including continuous or oscillating or pulsed flow or a flow profile with rest periods in the stimulation cycle [127]. Particularly with perfusion flow bioreactors, scaffold architecture must be taken into account, such as the size and interconnectedness of the porous network in the scaffold interior [144].

3 MATERIALS AND METHODS

3.1 Scaffold fabrication

The polymer composite scaffolds were fabricated at the Tampere University of Technology Department of Electronics and Communications Engineering with commercially available PLCL (PURASORB PLC-7015; Corbion Purac Ltd., Amsterdam, the Netherlands). In the melt extrusion fabrication process, 40 wt-% of β-TCP (Plasma Biotal Ltd.) of 100–300 µm granule size was added to the raw material. The inherent viscosity of the polymer composite was 1.6 dl/g and the weight average molecular weight 250 000 g/mol. The melt extruded polymer rods were treated with a supercritical CO_2 method to create a porous structure [111]. The treatment was performed in a custom-fitted supercritical CO_2 reactor system (Waters Operating Corporation, Milford, USA). The samples were manually cut. The cylindrical scaffold dimensions measured from dry scaffolds were on average 10 mm of diameter and 3 mm of height, and 0.236 cm^3 volume (Figure 13). The supercritical CO_2 fabricated tissue engineering scaffolds possessed complex irregular structure. The PLCL-β-TCP scaffolds had approximately 300–500 µm pore size and 58 % porosity which were determined earlier by micro-computer tomography (micro-CT) imaging (data not shown). For structure comparison experiments, some PLCL-β-TCP scaffolds with 7 channels of 1 mm of diameter (Figure 13C) were fabricated, with 1 channel in the middle of the cross-section area and 6 channels surrounding it symmetrically.

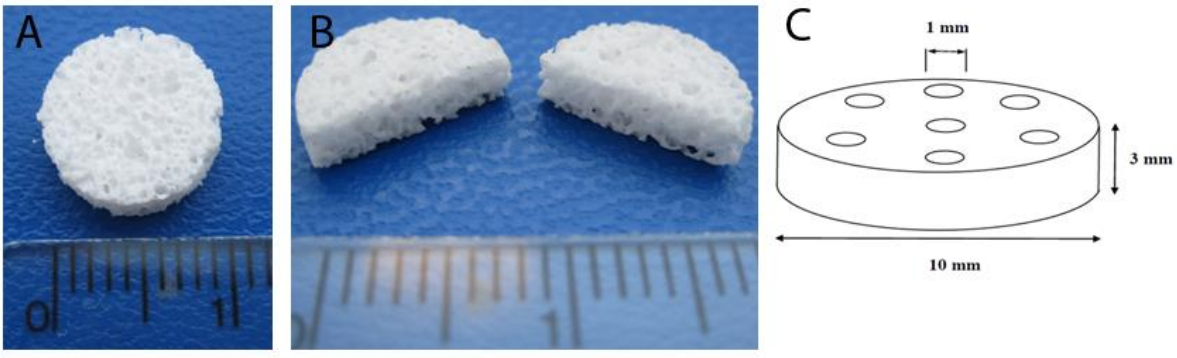

Figure 13. *Supercritical CO_2 fabricated PLCL-β-TCP tissue engineering scaffolds. A) Regular PLCL-β-TCP scaffold; B) Regular PLCL-β-TCP scaffold halved to show porosity; C) Schematic image of PLCL-β-TCP channel scaffold with 7x 1 mm diameter channels and scaffold dimensions. poly(L-lactic-co-ε-caprolactone)-β-tricalcium phosphate (PLCL-β-TCP).*

The tissue engineering scaffolds were gamma irradiated for sterility. A minimum irradiation dose of 25 kGy was applied by a commercial service supplier prior to the cell culture experiments. [172]

3.2 Bioreactor assembly

All the bioreactor parts must be suitable for aseptic cell culture work to avoid microbial contamination. To this end, the flow perfusion bioreactor system used in this study consisted of parts made of materials that were autoclavable. Autoclaving is a method to sterilize laboratory supplies by 20-min heat treatment at +121 ºC. All the cell culture and analyses were performed at the University of Tampere BioMediTech cell culture laboratories.

The flow perfusion bioreactor system (Figure 14) consisted of a polycarbonate culture chamber fabricated at the Tampere University of Technology Department of Electronics and Communications Engineering with commercially available polycarbonate, cell culture medium in a laboratory glass storage bottle, silicone hoses, custom-made stainless steel hose adapters, and a peristaltic pump (Heidolph PD 5101 pump drive with a peristaltic pump head SP Quick; Heidolph Instruments GmbH & Co. KG, Schwabach, Germany). The bottle screw cap was custom modified with 2 holes of 0.8 mm of diameter for the incoming and outgoing 0.8-mm silicone hoses as well as a gas-permeable 0.8/0.2 µm membrane filter for gas exchange (Acrodisc PF 32 mm Syringe Filter with Supor Membrane; Pall Life Sciences, Port Washington, WI, USA).

The bioreactor assembly was performed inside a cell culture laminar hood with sterile utensiles to avoid microbial contamination. In the bioreactor assembly (Figure 14), the culture chamber was assembled first on a support stand. The large silicone o-ring was placed in the large groove of the lower half of the culture chamber. The polycarbonate holder plate with 6 or 12 holes was placed in the middle of the chamber. The holder plate holes are spaced in a radial pattern. The presoaked and cell seeded cylindrical tissue engineering scaffolds measuring 10 mm in diameter and 3 mm in thickness were pressfitted to the holder plate holes prior to culture chamber assembly. The upper half of the culture chamber was tightened with 4 socket head stainless steel screws and an Allen key. The holes for the incoming and outbound hoses in the middle of the culture chamber were both fitted with a small silicone o-ring and a custom manufactured stainless steel nut with built-in adapter head.

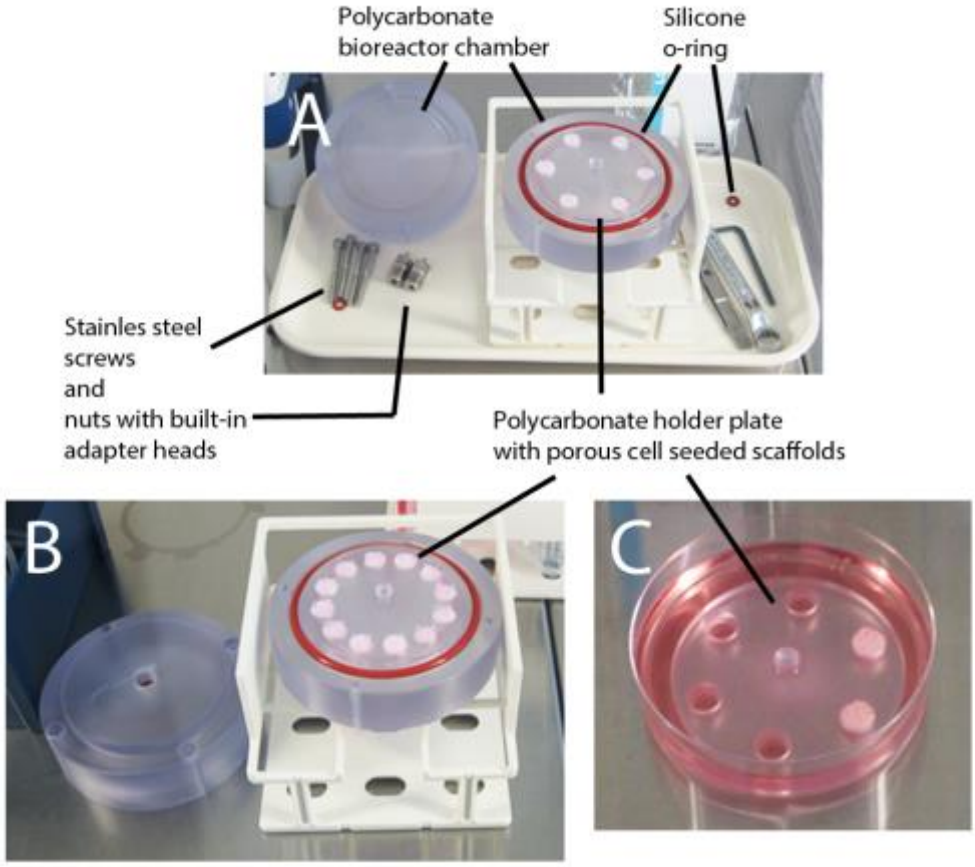

Figure 14. *The flow perfusion bioreactor assembly. Open bioreactor chamber with cell-seeded PLCL-β-TCP scaffolds in holder plates with A) 6 holes used for the flow rate of 0.50 mL/min/scaffold; B) 12 holes used for the flow rate of 0.25 mL/min/scaffold; C) Static controls in 6-holder plate in a Petri dish.*

The silicone pump hoses, 0.8 mm or 1.7 mm in diameter, were fitted with custom manufactured small or large, respectively, stainless steel adapters to attach the pump hose and the 1.0-mm silicone hose to the medium bottle and to the culture chamber to create a closed loop media system. In the medium bottle screw cap, the 1.0-mm silicone hoses were inserted through the cap holes for the incoming and outbound medium flow (Figure 14). The filter was placed on the bottle screw cap. The peristaltic pump drew medium from the bottle and perfused it through all scaffolds in bioreator chamber at a set rate. The unidirectional continuous fluid flow was directed axially through the porous cylindrical scaffolds orthogonally to the seeding surface, from top to bottom, to prevent air bubble accumulation under scaffolds that might alter the flow pattern on the surface of the scaffold [21]. The pumping speed was adjusted for 3 mL/min (0.50 mL/min/scaffold in 6-hole holder plate) according to pump manufacturer instructions and flow rates were also experimentally verified with or without scaffolds (data not shown).

To start the bioreactor system function, the culture chamber was filled with 0.3 ml/min/scaffold pumping speed for approximately 15 min and manually shaken to remove all air from inside the chamber. The polycarbonate chamber was semi-transparent

to observe filling. The overall flow rate was divided by the number of scaffolds to reach the actual flow rate of mL/min/scaffold. The medium reservoir and the reactor chamber were placed in a cell culture incubator with a 5 % CO_2 containing, +37 °C atmosphere of 80 % humidity. The total volume of medium in the flow system was 75 mL. The hoses passed through the incubator doors to the peristaltic pump (Figure 15).

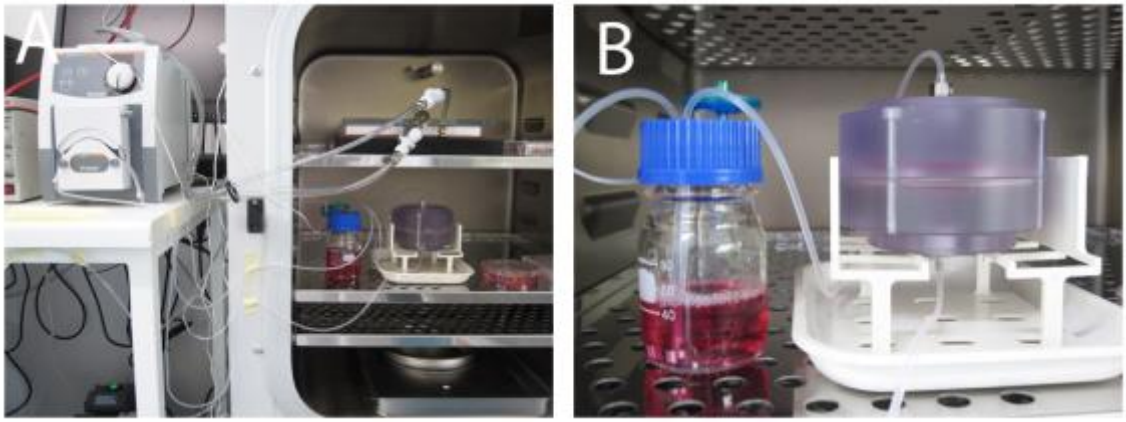

Figure 15. *The flow perfusion bioreactor culture circuit with A) Peristaltic pump outside incubator; B) Medium reservoir and bioreactor chamber inside incubator.*

Fresh medium was supplied by replacing the medium flask after one week of culture. This was done to provide hASCs with fresh nutrients and remove circulating debris or detached or dead cells from the system. In the tested flow perfusion bioreactor, a continuous steady fluid flow is directed through the porous scaffolds (Figure 16).

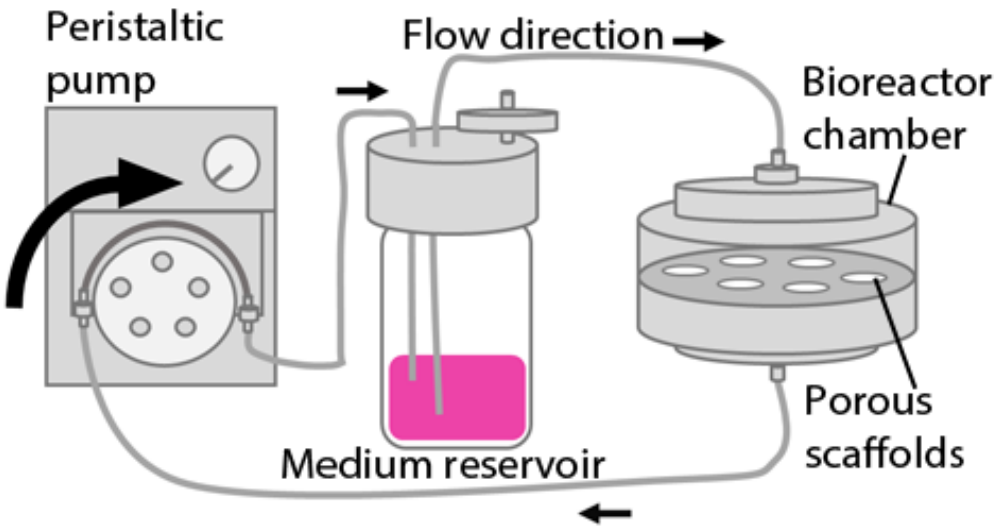

Figure 16. *Schematic presentation of the flow perfusion bioreactor system. The culture circuit used in the study with a peristaltic pump, continuous unidirectional fluid flow through a medium reservoir and a bioreactor chamber with porous scaffolds. Arrows indicate direction of pump rotation and fluid flow.*

The flow rate for the comparison experiment was adjusted by using the holder plates; 6-hole plate was used for the flow rate of 0.50 mL/min/scaffold and 12-hole plate was used for the flow rate of 0.25 mL/min/scaffold. The 6-hole and 12-hole holder plates were interchangeable for the culture chamber. In the design of the holder plate, the dimensions of the hole and the scaffold had tight tolerance to prevent nonperfusing flow.

3.3 Cell isolation, expansion and characterization

3.3.1 Adipose stem cell isolation and expansion

The hASCs were isolated from subcutaneous adipose tissue samples of 2 healthy female donors of 57±3 years of age. The adipose tissue samples were donated from Tampere University Hospital Department of Plastic Surgery surgeries with the patients' written informed consent. The hASCs isolation from adipose tissue samples was conducted in accordance with the Ethics Committee of Pirkanmaa Hospital District, Tampere, Finland (R15161). The hASCs isolation procedure has been described by Zuk and coworkers [51; 173]. The tissue sample hASC isolation procedure has been developed and optimized previously [72; 174]. In the mechanical and enzymatic isolation procedure, the adipose tissue were first minced with surgical equipment and digested with 1.5 mg/mL collagenase type I (Thermo Fisher Scientific Inc., Waltham, MA, USA) in maintenance medium (MM) containing GIBCO Dulbecco's Modified Eagle Medium/Ham's Nutrient Mixture F-12 (DMEM/F-12 1:1; Thermo Fisher Scientific Inc.), 5 % human serum (HS) (PAA Laboratories Gmbh, Pasching, Austria), 1 % L-glutamine (GlutaMAX; Thermo Fisher Scientific Inc.), and 1 % antibiotics/antimycotic containing 100 U/mL penicillin/100 U/mL streptomycin (P/S) (Thermo Fisher Scientific Inc.). After the enzymatic digestion, the obtained stem cells were pelleted by centrifugation at 1 800 rpm for 10 min (Heraeus Labrofuge 400R Centrifuge, Thermo Fisher Scientific Inc.) and any remaining cellular debris was removed by filtration. The expansion of hASCs was carried out in T-75 polystyrene flasks (Nunclon Δ Surface, Sigma-Aldrich, St. Louis, MO) in MM and in a 5 % CO_2 containing, humidified +37°C atmosphere. The cells were passaged at 80 % confluence with TrypLE Select (Thermo Fisher Scientific Inc.). The expanded hASCs were cryopreserved in freezing solution of HS (PAA Laboratories Gmbh) containing 10 % dimethyl sulfoxide (Hybri-Max; Sigma-Aldrich) in liquid nitrogen and thawed for initial expansion for experiments in MM.

Prior to cell seeding, the polymer scaffolds were pretreated for 48 h in MM. The bioreactor parts were washed and autoclaved prior to each experiment. The hASCs were plated at a density of 153 000 cells/cm^2 in a volume of 50 µL. The cell seeded scaffolds were incubated for 3 h after plating at +37 ºC to allow cell attachment. The dynamic cell culture was initiated 24 h after plating by starting the continuous unidirectional perfusion flow with the peristaltic pump. The control cell cultures in static condition were kept on holder plates in a Petri dish, and blank samples in 48-well plate wells (Nunclon), and both

were maintained in MM, changed every other day. The experiments were carried out at hASC passage 5.

3.3.2 Cell characterization

Flow cytometry was used to characterize hASC cell surface markers. Briefly, the hASCs of passage 1–2 were analyzed for cell surface markers with fluorescence activated cell sorter (FACS) (FACSAria; BD Biosciences, San Jose, CA, USA).

The mesenchymal origin of hASCs was verified by the expression of cell differentiation marker profile with monoclonal antibodies against CD3-PE, CD14-PE-Cy7, CD19-PE-Cy7, CD45RO-APC, CD54-FITC, CD73-PE, CD90-APC (BD Biosciences), CD11a-APC, CD80-PE, CD86-PE, CD105-PE (R&D Systems, Inc., Minneapolis, MN, USA), CD34-APC and HLA-DR (Immunotools GmbH, Friesoythe, Germany). FACS analysis was performed on 10 000 cells per sample, and the positive expression was defined as a level of fluorescence 99 % greater than the corresponding unstained cell sample [175].

3.4 Cell viability

The cell viability was analyzed using Live/Dead fluorescence staining (Thermo Fisher Scientific Inc.). Briefly, after washing in Dulbecco's phosphate-buffered saline (DPBS) (Thermo Fisher Scientific Inc.), the samples were incubated for 45 min at room temperature with a mixture containing 0.5 mM calcein acetoxymethyl ester (Calcein AM) (Thermo Fisher Scientific Inc.) to detect viable cells at 488 nm. Solution of 0.25 mM ethidium homodimer-1 (EthD-1) (Thermo Fisher Scientific Inc.) was used to detect necrotic cells at 560 nm.

The images of the viable green fluorescent cells and the necrotic red fluorescent cells were taken using an epifluorescence microscope (Olympus IX51, Olympus Finland PLC, Vantaa, Finland). The image brightness and contrast was adjusted manually (Adobe Photoshop CS4, San Jose, CA, USA).

3.5 Cell number and proliferation

Cell number was determined with CyQUANT Cell Proliferation Assay Kit (Thermo Fisher Scientific Inc.) at 1-, 7-, or 14-day time points. Briefly, the cells were lysed with 0.1 % Triton X-100 buffer (Sigma-Aldrich) and stored at –80°C. The quantitative alkaline phosphatase activity (qALP) was analyzed from the same lysates.

Upon analysis, working solution for each sample was prepared with CyQUANT GR Dye in dimethyl sulfoxide (Thermo Fisher Scientific Inc.) together with Cell Lysis Buffer (Thermo Fisher Scientific Inc.). The blue-green fluorescence of 3 parallel samples was measured with a microplate reader (Victor 1420 Multilabel Counter; PerkinElmer,

Waltham, MA, USA) at 480/520 nm. In the results' analysis, the background of static blank acellular samples was subtracted from the cell experiment sample values.

3.6 Osteogenic differentiation

3.6.1 Alkaline phosphatase activity

The qALP (ALP Kit; Sigma-Aldrich) activity was analyzed at 1, 7, or 14 days. The qALP was analyzed from the same cell lysate samples as the cell number in the following thawing of samples. The absorbance was measured at 405 nm with microplate reader (Victor 1420 Multilabel Counter; PerkinElmer). In the qALP analysis, the hydrolysis of p-nitrophenyl phosphate is catalyzed by ALP enzyme in alkaline solution. The hydrolysis releases yellow colored p-nitrophenol. The rate of p-nitrophenol formation is proportional to the sample's catalytic concentration of ALP.

3.6.2 Total collagen

Total collagen content was analyzed at 7-day time point using a quantitative Sircol Soluble Collagen Assay (Biocolor Ltd., Carrickfergus, Northern Ireland). In brief, the acid soluble collagen was extracted from scaffolds with 0.1 mg/mL pepsin from porcine gastric mucosa (Sigma-Aldrich) in 0.5 M acetic acid (Merck KGaA, Darmstadt, Germany).

Sircol Dye reagent (Biocolor Ltd.), which contains Sirius Red and picric acid, was added to the samples and incubated for 30 min to allow the collagen to form a red complex with the dye. The collagen-dye pellet was washed to remove any unbound dye and an alkali reagent of 0.5 M NaOH solution (Biocolor Ltd.) was added in order to resolubilize the collagen. Finally, the intensity of red dye of 2 technical parallel samples was measured with a microplate reader at 540 nm (Victor 1420 Multilabel Counter; PerkinElmer). In the results' analysis, the background of static blank samples was subtracted from the results.

3.6.3 Mineralization

Cellular mineralization was measured with a quantitative Alizarin Red S (Sigma-Aldrich) at 14-day time point. Briefly, the cells were rinsed with DPBS, after which cells were fixed with 4 % paraformaldehyde (PFA) (Sigma-Aldrich) for 35 min. The PFA fixed samples were washed with dH_2O. The samples were stained with 2 % Alizarin Red S (Sigma-Aldrich) of pH 4.2 and incubated for 10 min. After dH_2O and 70 % ethanol washes, the dye was extracted with 100 mM cetylpyridinium chloride (Sigma-Aldrich) in gentle shaking for 3 h.

The purple dye intensity of 3 technical parallel samples was determined immediately using a microplate reader (Victor 1420 Multilabel Counter; PerkinElmer) at 540 nm.

3.7 Experimental design

This study consisted of a number of preliminary experiments before proceeding to actual full length experiments of, firstly, flow rate comparison and, secondly, scaffold structure comparison (Table 3). In the flow rate comparison, 2 different flow rates of 0.25 and 0.50 mL/min/scaffold were compared for hASC stimulation based on literature review (Table 2). In the scaffold structure comparison, a modified PLCL-β-TCP scaffold pierced with punctured channels was compared to the unmodified regular structure with irregular porosity fabricated with the supercritical CO_2 method with the selected flow rate. Only single experiment repeats were performed for both experiments with hASCs from 2 different donors (Table 3).

The number of samples analyzed at each indicated time point is presented for each method of analysis. The risk of microbial contamination was monitored with BacT/ALERT detection system (bioMérieux, Durham, NC, USA) from cell culture medium samples by the Regea Cell and Tissue Center Quality Management services.

Table 3. *Experimental design.*

Experiment	hASCs	Condition and time	Scaffold	Flow rate [mL/min/ scaffold]	Live/Dead viability	CyQUANT cell number	qALP	Total collagen content	Alizarin Red S mineralization
Flow rate comparison	Donor 1	Dynamic 14 d	Regular PLCL-TCP40	0.25	3x 14 d	3x 14 d	3x 14 d	3x 14 d	3x 14 d
		Static 14 d	Regular PLCL-TCP40	--	3x 14 d	3x 1 d, 3x 14 d	3x 14 d	3x 14 d	3x 14 d
	Donor 1	Dynamic 14 d	Regular PLCL-TCP40	0.50	2x 14 d	2x 14 d	2x 14 d	2x 14 d	--
		Static 14 d	Regular PLCL-TCP40	--	3x 14 d	2x 1 d, 3x 14 d	3x 14 d	3x 14 d	--
Scaffold structure comparison	Donor 2	Static 7 d +Dynamic 7 d	Channel PLCL-TCP40	0.50	2x 14 d	2x 14 d	2x 14 d	--	2x 14 d
		Static 14 d	Channel PLCL-TCP40	--	--	1x 7 d, 1x 14 d	1x 7 d, 1x 14 d	--	1x 14 d

Abbreviations: *hASC, human adipose stem cells; PLCL-TCP40, Poly(L-lactic-co-ε-caprolactone) with 40 wt-% of beta-tricalcium phosphate; qALP, quantitative alkaline phosphatase activity.*

4 RESULTS

Different flow rates and scaffold structures were compared to analyze the effect on hASC viability, proliferation, and osteogenic differentiation in the new flow perfusion bioreactor and in the novel supercritical CO_2 fabricated PLCL-β-TCP scaffolds.

The isolated hASCs were initially characterized by flow cytometry. Cell viability, morphology, and adhesion were observed qualitatively with Live/Dead staining. Cell number based on the total amount of DNA was analyzed at different time points to determine cell proliferation quantitatively. Osteogenic differentiation of hASCs was studied quantitatively by qALP, total collagen content, and mineralization of the formed ECM.

4.1 Cell characterization

The flow cytometric cell surface marker expression analysis was used for the characterization of the hASCs and performed in passage 5 for both donors after expansion in MM (Table 4).

Table 4. *Flow cytometric cell surface marker profile of the hASC donors 1 and 2 compared to International Society for Cellular Therapy (ISCT) established criteria. Data is expressed as mean and standard deviation (SD).*

Surface protein	Mean	SD	ISCT criteria
3	0,3	0,1	
11a	0,4	0,4	
14	0,8	1,0	2
19	0,5	0,5	2
34	5,5	4,0	2
45	1,1	0,4	2
54	3,1	1,4	
73	74,9	8,0	95
80	0,5	0,4	
86	0,7	0,6	
90	99,5	0,4	95
105	90,0	6,8	95
HLA-DR	0,8	0,8	2

No bacterial contaminations were detected during this study according to the BacT/ALERT microbial detection system results, measured and reported by the Regea Cell and Tissue Center Quality Management services (data not shown).

4.2 Cell viability

The hASC viability and adhesion were evaluated using Live/Dead fluorescence staining at 14-day time point. In the flow rate comparison experiment dynamic condition, the hASCs were perfused continuously with a steady flow rate of either 0.25 or 0.50 mL/min/scaffold for 14 days (Figure 17A;B), whereas in the scaffold structure experiment dynamic condition, the hASCs were precultured in static condition for 7 days prior to 7 days of continuous perfusion flow with a flow rate of 0.50 mL/min/scaffold (Figure 17C).

The scaffolds were cut in half to visualize cell viability and distribution interior the porous structure (Figure 17). The samples were imaged immediately after staining with an epifluorescence microscope.

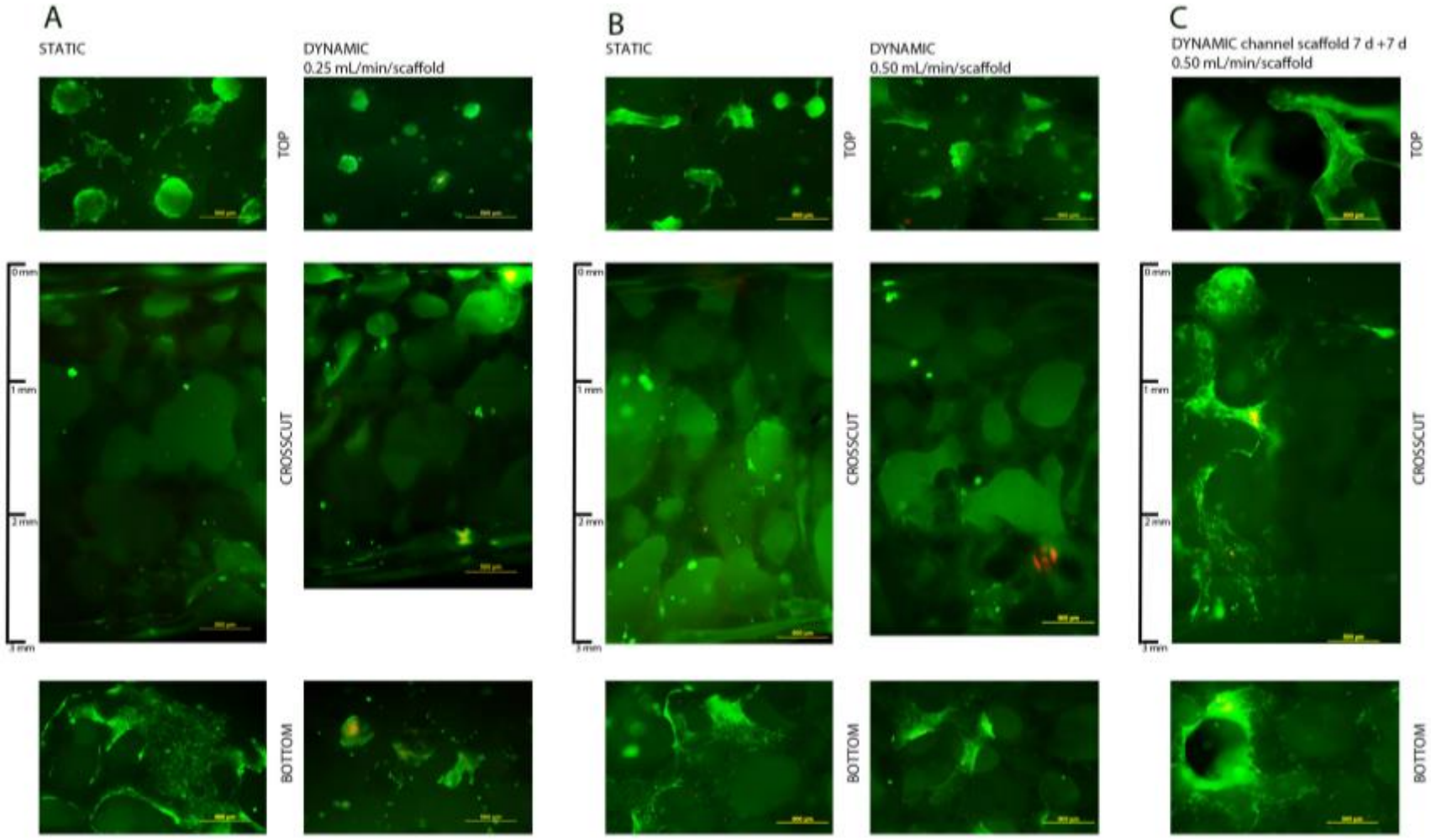

Figure 17. *Cell viability. Live/Dead staining at 14 days of viable Calcein AM stained (green fluorescence) and dead EthD-1 stained (red fluorescence) hASCs in A) Regular PLCL-β-TCP scaffolds in static and dynamic conditions with flow rate of 0.25 mL/min/scaffold; B) Regular PLCL-β-TCP scaffolds in static and dynamic conditions with flow rate of 0.50 mL/min/scaffold; C) In PLCL-β-TCP channel scaffolds in dynamic culture with flow rate of 0.50 mL/min/scaffold after 7 d preculture followed by 7 d flow perfusion. Original magnification 40×, scale bar 500 μm.*

4.3 Cell proliferation

Cell number and proliferation of the hASCs in the dynamic and in static conditions was analyzed based on the quantitative measurement of DNA content at 1-, 7-, or 14-day time points (Figure 18). All results are relative to the static condition due to the fact that it was possible to collect samples only from the static culture during experiment because the bioreactor chamber and the cell culture loop had to remain intact until the end of the experiment to avoid microbial contamination.

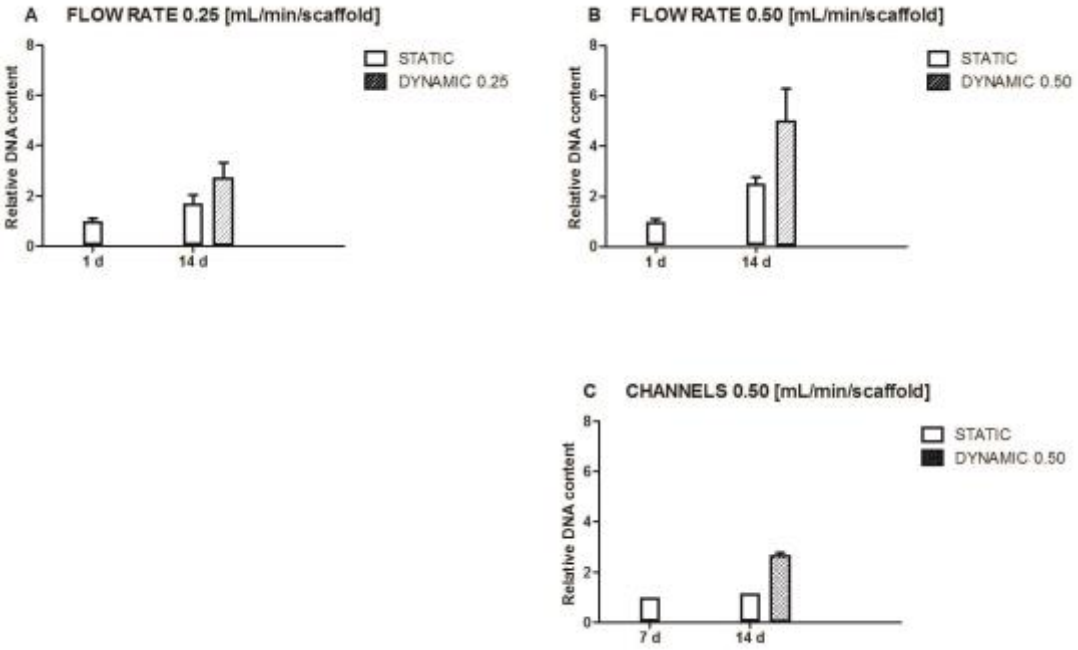

Figure 18. Cell proliferation. *Relative DNA content*
A) In regular PLCL-β-TCP scaffolds in dynamic and in static condition measured at 1- and 14-day time points. Flow rate 0.25 mL/min/scaffold. Results are relative to static condition at 1-day time point;
B) In regular PLCL-β-TCP scaffolds in dynamic and in static condition measured at 1- and 14-day time points. Flow rate 0.50 mL/min/scaffold. Results are relative to static condition at 1-day time point;
C) In PLCL-β-TCP channel scaffolds in dynamic and in static condition measured at 7- and 14-day time points. Flow rate 0.50 mL/min/scaffold. Results are relative to static condition at 7-day time point.
Data is expressed as mean and standard deviation. PLCL-β-TCP, poly(L-lactic-co-ε-caprolactone)-β-tricalcium phosphate.

In the flow rate comparison for the regular PLCL-β-TCP scaffolds, the hASC proliferation results for the dynamic condition with 0.25 mL/min/scaffold flow rate was 1.6× fold higher compared to the static control and 2.0× fold higher with 0.50 mL/min/scaffold flow rate. In the structure comparison, the dynamic condition had 2.3× fold higher hASC proliferation in the channel PLCL-β-TCP scaffolds compared to the

static control at 14 days (Table 5). The highest hASC proliferation result was measured for the channel PLCL-β-TCP scaffolds after the 7-day preculture and 7-day culture at 0.50 mL/min/scaffold flow rate compared to the static control at 14 days.

Table 5. *The cell proliferation results for different dynamic conditions compared to the static controls at 14 days.*

	Flow rate [mL/min/scaffold]	**Scaffold**	**Higher cell proliferation in dynamic condition [%]**
Flow rate comparison	0.25	regular	160
	0.50	regular	200
Structure comparison	0.50	channel	230

4.4 Osteogenic differentiation

To determine hASC osteogenic differentiation, qALP, total collagen content and ECM mineralization were measured. The mineralization results were qualitative when the scaffolds were imaged by a digital camera, and quantitative when the staining was extracted and its absorbance measured, see Subchapter 4.4.3.

4.4.1 Alkaline phosphatase activity

The qALP of hASCs in the dynamic and static condition was analyzed at 1-, 7-, or 14-day time points for the flow rate and structure comparison experiments (Figure 19) from the same sample lysates analyzed for DNA content in CyQUANT analysis in Subchapter 4.3.

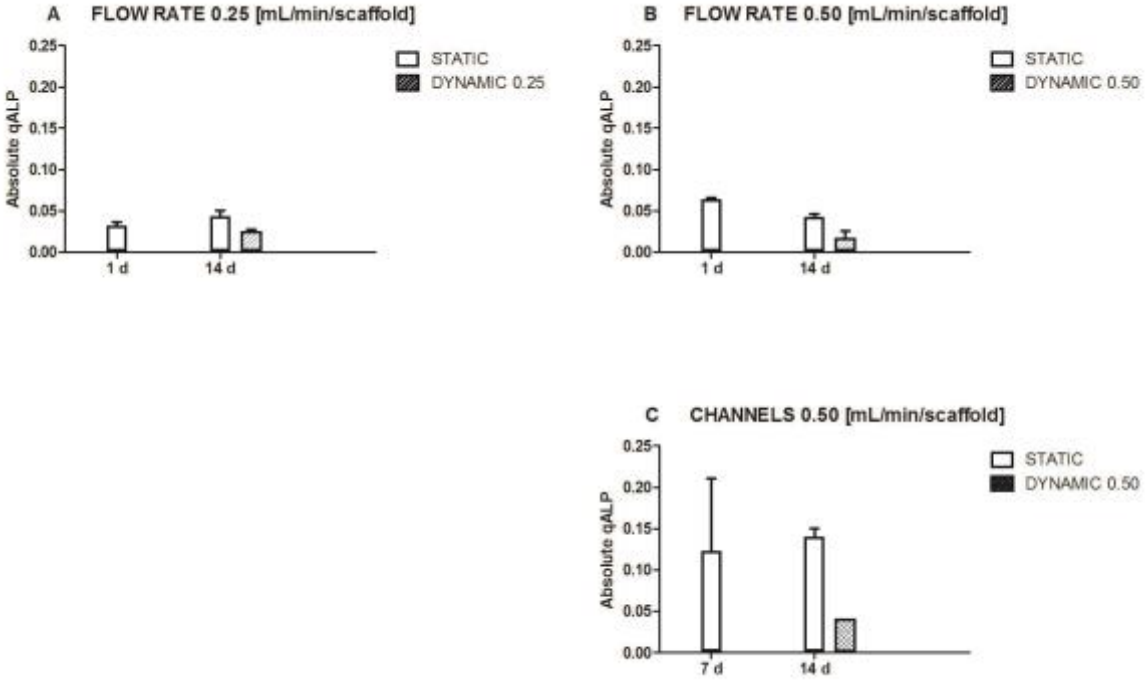

Figure 19. *Absolute quantitative alkaline phosphatase activity (qALP) results.*
A) In regular PLCL-β-TCP scaffolds in dynamic and in static condition measured at 1- and 14-day time points. Flow rate 0.25 mL/min/scaffold. Results are relative to static condition at 1-day time point;
B) In regular PLCL-β-TCP scaffolds in dynamic and in static condition measured at 1- and 14-day time points. Flow rate 0.50 mL/min/scaffold. Results are relative to static condition at 1-day time point;
C) In PLCL-β-TCP channel scaffolds in dynamic and in static condition measured at 7- and 14-day time points. Flow rate 0.50 mL/min/scaffold. Results are relative to static condition at 7-day time point.
Data is expressed as mean and standard deviation. PLCL-β-TCP, poly(L-lactic-co-ε-caprolactone)-β-tricalcium phosphate.

Only 1 sample was available for the structure comparison experiment's static condition 7-day time point due to shortage of scaffolds. The absorbance results below 0.25 at 405 nm were overall very low and close to blank values.

4.4.2 Total collagen

The total collagen content of the 14-day time point samples was measured using a quantitative Sircol Soluble Collagen Assay (Figure 20) and normalized to cell number based on the DNA content results, shown in Subchapter 4.3. Due to material shortage of channel scaffolds, only regular scaffolds were analyzed for total collagen content. The results for both the flow rates and structures in the dynamic condition were equally low or lower compared to static control at 14 days.

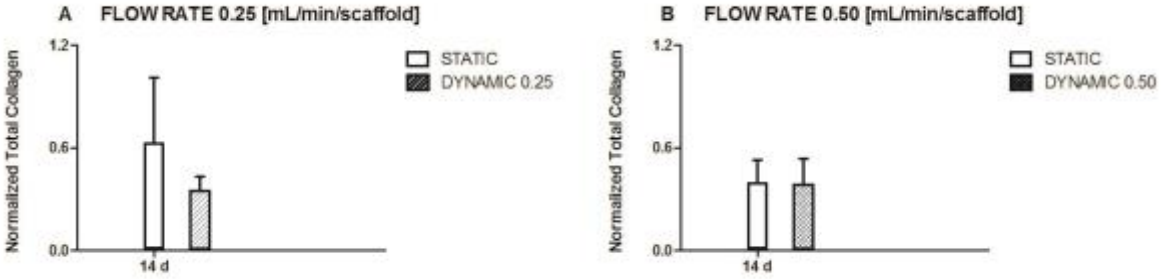

Figure 20. *Normalized total collagen content.*
A) In regular PLCL-β-TCP scaffolds in dynamic and in static condition measured at 14-day time point. Flow rate 0.25 mL/min/scaffold. Results are relative to static condition;
B) In regular PLCL-β-TCP scaffolds in dynamic and in static condition measured at 14-day time point. Flow rate 0.50 mL/min/scaffold. Results are relative to static condition. Data is expressed as mean and standard deviation. PLCL-β-TCP, poly(L-lactic-co-ε-caprolactone)-β-tricalcium phosphate.

4.4.3 Mineralization

The calcium deposits of sample cells' mineralized ECM was quantified at 14-day time point with a quantitative Alizarin Red S assay (Figure 21). Due to material shortage of channel scaffolds, only 1 static channel scaffold was analyzed for the mineralization assay. The qualitative staining results of the mineralization assay prior to quantitative stain extraction are shown below (Figure 22).

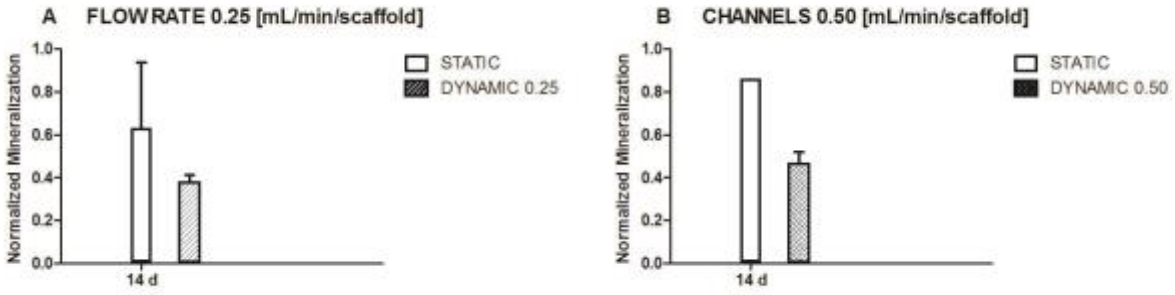

Figure 21*. Normalized mineralization.*
A) In regular PLCL-β-TCP scaffolds in dynamic and in static condition measured at 14-day time point. Flow rate 0.25 mL/min/scaffold. Results are relative to static condition;
B) In PLCL-β-TCP channel scaffolds in dynamic and in static condition measured at 14-day time point. Flow rate 0.50 mL/min/scaffold. Results are relative to static condition. Data is expressed as mean and standard deviation. PLCL-β-TCP, poly(L-lactic-co-ε-caprolactone)-β-tricalcium phosphate.

The calcium component of the PLCL-β-TCP composite caused some background. This is seen in the blank sample staining (Figure 22), and its quantitated value was subtracted from the measured results.

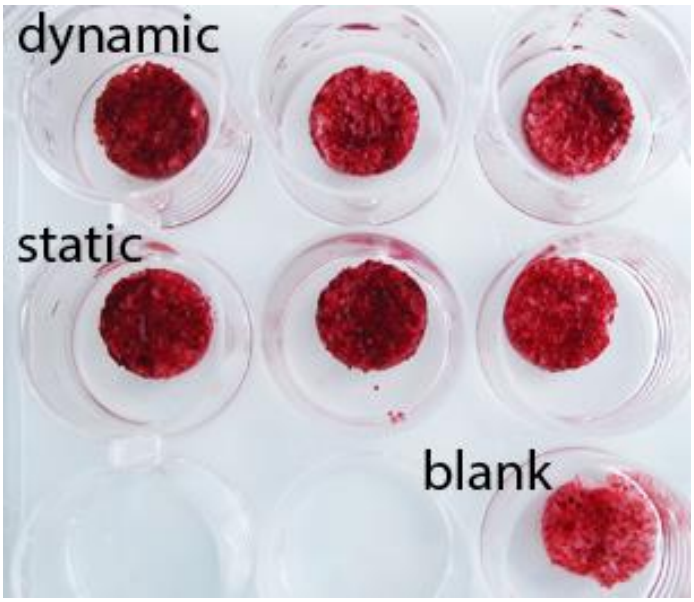

Figure 22. *Alizarin Red S staining. Mineralized calcium deposits from hASCs cultured in PLCL-β-TCP scaffolds under 0.25 mL/min/scaffold flow and in static condition, and blank control analyzed at 14-day time point.*
hASCs, human adipose stem cells; PLCL-β-TCP, poly(L-lactic-co-ε-caprolactone)-β-tricalcium phosphate.

Additionally, pH of both the dynamic and static condition culture media was measured at 14-day time point for regular PLCL-β-TCP scaffolds only for the 0.50 mL/min/scaffold flow rate experiment. The measured value of the dynamic condition was pH 8.8 and for the static condition it was pH 8.5.

5 DISCUSSION

There were no significant differences between the results in any of the tested experiment conditions. The objectives of this study as well as the different factors and also experiment validity and reliability that possibly contributed to these results are discussed in the following chapters.

5.1 Cell characterization, viability and morphology

Cell characterization

The hASCs used in the study expressed the surface markers CD73, CD90 and CD105, whereas the cell surface markers CD34 and CD54 showed only moderate expression, and CD3, CD11a, CD14, CD19, CD45, CD80, CD86 and HLA-DR were not expressed (Table 4). The analyzed cell surface marker profile included hematopoietic markers CD34 and CD45 as negative controls and of which CD34 was somewhat elevated, however, this is probably due to the low passage 1–2 of the analyzed hASCs and typically seen when HS is included in the cell culture medium. Therefore, the higher CD34 result can be expected to decrease with higher passage values [176; 177]. The FACS results showed that the hASC CD marker profile was in line with the ISCT established criteria [49] which confirmed the mesenchymal origin of the hASCs used in the experiments.

Cell viability and morphology

The living cells were stained green and dead cells were visible in red after the staining. In the flow rate comparison static condition, the hASCs were well viable and spread out (Figure 17A;B), eventhough the donor 1 hASCs typically showed tendency to form aggregates in all the experiments. The cells adhered well and grew mostly on the scaffold periphery in the static condition and there were only some individual cells visible in the crosscut image (Figure 17B) in the absence of larger cell aggregates. In the dynamic conditions, there were some dead cells which were visible in yellow in the Live/Dead images, but there was not any considerable difference in cell viability or morphology between the different flow rates tested (Figure 17A;B). There were hASCs growing also on the bottom surface of the scaffolds, and therefore it can be concluded that the fluid flow had diffused cells through the structure and ensured their viability. However, the perfusion flow did not perceivably enhance homogeneous cell distribution in the scaffold volume, because there was not any considerable amount of cells stained in scaffold crosscut images of the dynamic condition compared to the static control (Figure 17A;B). Cell morphology was typically rounded in the dynamic condition, and the perfusion flow

enhanced the formation of densely packed cell aggregates which were tighter in the appearance compared to the static control regardless of donor 1 hASC associated tendency to form aggregates. This phenomenon was also observed with hASCs from a different donor and indicated that the tight cell aggregates and round morphology are characteristic effects caused by flow perfusion stimulation. Similarly, Bjerre et al. (2011) noted that even a 7-day static preculture could not rescue hBMSC morphology after a 7-day 0.1 mL/min/scaffold perfusion which resulted in rounded cells without focal adhesions. On the contrary, the hASCs formed uniform layers in the static condition, where the cells were able to spread out especially onto the top seeding surface. [16]. Baumgartner et al. (2015) also reported round hASC morphology under perfusion in PLGA-CaP scaffolds but only for higher 2.0 mL/min/scaffold flow rates, whereas at 0.3 and 0.5 mL/min/scaffold flow rates the hASCs retained an elongated morphology [37]. This difference might be partly caused by donor variation or differences in fluid flow properties interior the different types of scaffolds.

In the scaffold structure comparison dynamic condition, the hASCs were mostly viable in regular scaffolds eventhough some dead cells were seen in the larger cell aggregates (Figure 17C), however, this was expected due to lack of space, oxygen, or nutrients in the inner parts of aggregates. Cell morphology was more elongated with the 7-day preculture prior to the 7-day perfusion flow compared to the 14-day steady continuous flow (Figure 17B;C). In the channel scaffolds in the dynamic condition, the hASCs were able to migrate through the scaffold interior along the pore walls and distributed homogeneously through the entire scaffold cross-section, however, there were no cells seen outside of the channels (Figure 17C). This indicates that the perfusion flow was directed through the channels and that it did not diffuse through the surrounding irregular pores of the scaffold bulk material. In the static condition in the regular scaffolds, there were large cell aggregates of mostly viable cells on the scaffold periphery and some individual dead cells in the interior of the scaffolds (Figure 17B).

Generally, one prerequisite of hASC osteogenic differentiation is the cell ability to adhere and spread out onto a surface [178]. This was clearly not the case under dynamic perfusion flow, where the hASCs remained in tightly rounded morphology. Spread out cell morphology could be a key switch to hASC osteogenesis to be tested in future experiments, because hASC have been reported to adapt cuboidal osteoblast-like morphology upon osteogenic differentiation [33]. On the contrary, rounded cell morphology of osteocyte-like cells has been linked to higher mechanosensitivity compared to adhered and flattened morphology [179]. Still, these Live/Dead results show the good cytocompatibility of the PLCL-β-TCP scaffolds.

5.2 Cell distribution

Generally, in the dynamic flow perfusion condition, the cells were slightly more evenly distributed throughout the scaffold volume, whereas in the static condition the cells grew as a thick layer mostly on the scaffold periphery. However, the difference in cell distribution was not considerable and penetration of hASCs through the depth of the regular PLCL-β-TCP scaffolds was less pronounced than what was hypothesized. The dense cell sheet on scaffold surface subsequently blocks diffusion of oxygen and nutrients or removal of debris from any cells attempting to grow deeper into the structure. In the dynamic condition, there were only some narrow passages visible in each crosscut where there were some individual cells across the whole scaffold cross-section which proved the scaffold structure porosity and pore interconnectedness at least in some parts of the structure. This effect might be due to the irregular structure and varied porosity of the PLCL-β-TCP scaffolds. This result was therefore partly consistent with a previous studies demonstrating usefulness of flow perfusion bioreactors for homogenous cell distribution of critical size bone constructs. Bjerre et al. (2008) gained homogeneous distribution of hBMSCs and cell matrix in silicate-TCP with continuous 0.1 mL/min/scaffold flow rate [15], whereas Fröhlich et al. (2010) reported more homogeneous cell distribution and bone ECM production of BSP, OP, COL1 after 5 weeks in osteogenic medium (OM) perfusion with continuous 0.3 mL/min flow rate in decellularized bone [36]. In similar terms to results of the current study, nonhomogeneous cell distribution under perfusion has been noted also in other studies [180].

In the static condition, some of the seeded cells usually drip straight through the scaffold structure and adhere to the well bottom of the polystyrene well plate and then gradually grow back onto the scaffold upwards from the well bottom. This might result into falsely higher cell numbers for the static condition eventhough upon analysis the scaffolds are moved individually to new wells. To overcome this bias in these experiments, the static condition was plated on a similar holder plate and cultured in a Petri dish to prevent cell growth from the bottom of the plate back onto the scaffold. Therefore, the results of the static control condition were considered reliable.

The homogeneity of the cell distribution was somewhat unclear because the cells inside the structure were only faintly stained and the sensitive fluorescent signal was easily extinguished upon closer inspection and there was only little time to focus the image. In addition, the composite material caused some autofluorescence background in the images. Indeed, PCL autofluorescence has been reported to interfere with cell viability imaging in 3D scaffolds [32]. In the Live/Dead assay, the cells in the inner parts of the scaffolds seemed only weakly stained despite the fact that some scaffolds were halved prior to staining. The incubation was performed in static condition instead of the usual gentle shaking because the rounded cells seemed to detach easily from the scaffolds. Compromised scaffold permeability might have affected staining results by partly

blocking the inflow of the staining solution. In addition, the PLCL-β-TCP scaffold material was optically dense and due to its opacity, only the few cells present in the random crosscut plane were observed. Only single random crosscut of each sample scaffold was imaged. What is more, the scaffolds were cut manually with a scalpel blade and some cells observed in the plane of the crosscut might have originated from the scaffold surface and been transferred along the cutting blade. In the future, a more homogeneous cell distribution inside the structure might be achieved with dynamic cell seeding. In addition, more sensitive and higher resolution imaging methods are called for to visualize cells more clearly inside the porous structures.

5.3 Cell number and proliferation

In the flow rate comparison, the flow rate of 0.50 mL/min/scaffold increased hASC proliferation at 14 days (Figure 18B) and, therefore, it was selected for further flow perfusion experiments in the structure comparison. Consistently, an earlier study reported that the 0.50 mL/min flow perfusion increased significantly cell proliferation compared to the static control in similar porous polymer scaffolds [143]. Perfusion flow has also previously been reported to increase cell proliferation [21; 137; 167; 181; 182]. Similarly, for hASCs, higher proliferation but weak osteogenic differentiation in MM in BaG foam scaffolds was noted by Silva et al. (2014) in continuous 0.1 mL/min/scaffold perfusion culture [33].

In the scaffold comparison, the hASC proliferation was higher in the dynamic condition in the channel scaffolds (Figure 18C). This might be due to the 7-day preculture of the hASCs in the channel scaffolds before submitted to perfusion flow and different fluid shear stress in the channels. However, only 1 sample was available for analysis in the static condition in the scaffold structure comparison to relativise the results and these results might need to be verified by further experiment repeats.

The irregular porous structure seemed at times challenging to handle during the incubations and sample collection when some of the liquid might have been retained inside the pores or might not have penetrated the pores at all. Despite this, cell proliferation was considerably higher in the all dynamic conditions compared to the static controls and the trend was clearly recognazible in all the experiments. Based on this, the results were repeatable and valid and the analysis method reliable. Therefore, the flow perfusion bioreactor can be used as a method to increase cell number and possibly even a more homogenous cell distribution in the scaffold volume.

5.4 Osteogenic differentiation

Overall, the results for hASC osteogenic differentiation failed to confirm the hypothesis that perfusion flow in porous osteoconductive PLCL-β-TCP scaffolds would promote

bone ECM formation. In this study, the culture duration of 2 weeks might not have been sufficient to evaluate late osteogenic markers or bone-matrix deposition when late osteogenic proteins such as OC or RUNX2 which have been previously reported to require at least 3 weeks to evolve [136]. The following chapters detail the different parameters that contributed to these results and what might be possible solutions to some of these issues.

5.4.1 Alkaline phosphatase activity

The qALP results normally increase with increasing cell number [183] to reach absorbance values typically between 0.5–2.0 at 405 nm for strong osteogenic induction [184], but the results for the higher proliferation rate experiment condition of 0.50 mL/min/scaffold flow rate comparison decreased in time (Figure 19B). The higher cell proliferation in the dynamic condition compared to the static control in both the experiments might have caused low qALP results because the hASCs might have been in the proliferation phase instead of differentiation phase. Nevertheless, both the results were close to the blank result with an absolute absorbance value approaching 0.05 at 405 nm. In addition, the results for 0.25 mL/min/scaffold flow rate were equally low and, therefore, the qALP results for the flow rate comparison in regular PLCL-β-TCP scaffolds were close to zero results (Figure 19A;B). The only real albeit weak qALP result was obtained for the static condition at 14 days at the absolute absorbance value of 0.15 at 405 nm in the channel PLCL-β-TCP scaffolds. Similarly, Altman et al. (2014) reported that qALP was considerably downregulated under perfusion [80]. On the contrary, under pulsatile 0.008 mL/min/scaffold perfusion flow in OM in porous PCL scaffolds, qALP result of osteoblastic cells increased significantly up to 28 days compared to static control [32]. Rodrigues et al. (2012) reported significantly higher qALP results compared to static control for hASCs under 0.1 mL/min/scaffold flow at 14 days in MM [35]. In a recent study by Kleinhans et al. (2015), hMSC osteogenic induction in PLCL scaffolds was produced by 7-day fluid flow stimulus in MM [163].

It should also be taken into consideration that qALP might have peaked at a different time than the measured timepoints of 1, 7, or 14 days [184], however, it is generally considered an early osteogenic marker. Furthermore, a sufficient level of qALP for the mineralization to occur has not been determined. In comparison, in previous studies with BMSCs, flow perfusion has been shown to significantly increase qALP levels under perfusion conditions compared to static control [28; 185]. It is equally worth to note that whereas we applied continuous steady flow through the scaffolds, oscillatory flow, in comparison, has been reported to increase DNA amount and qALP over unidirectional continuous flow [136]. Overall, in our results, there was no indication of early osteogenic differentiation at the analyzed time points.

5.4.2 Total collagen

The applied Sircol collagen assay detects collagen types I–V, of which COL1 mostly constitutes bone matrix. Usually, collagenous matrix formation is required for the hASC osteogenic differentiation [183]. In the flow rate comparison, the total collagen content results for the same donor 1 were at a similar level at both flow rates. In the dynamic condition, the cell morphology remained tight and rounded and the hASCs formed tight aggregates and there was no visible accumulation of collagenous matrix. This may be due to harsh flow conditions because in other studies with increased collagenous ECM production under perfusion flow, hASCs were subjected to a maximum of 0.1 mL/min flow [186]. The addition of OM in combination with the β-TCP containing polymer composite scaffolds to the dynamic culture might improve the total collagen content. Furthermore, according to published research, cells have secreted more collagenous and osteogenic ECM after an initial fluid flow stimulation period [159; 160]. Optimal flow rates and culture conditions could be optimized further to encourage production of collagen rich ECM and subsequently to form a more mature bone-like construct.

5.4.3 Mineralization

The mineralization result normalized to cell number was lower for the dynamic condition than for the static controls in the regular scaffolds for donor 1 hASCs, and the results for the channel PLCL-β-TCP scaffolds with donor 2 hASCs followed the same trend. This result failed to confirm the hypothesis that preculture would enhance ECM production and subsequently its mineralization. In the experiment with channel scaffolds, the samples were precultured for 1 week before starting the bioreactor culture. The hypothesis was that this would have allowed initially the collagenous ECM to form and to be subsequently mineralized by the stimulus provided by the fluid flow shear stress. It was also predicted that the preculture might also dampen the harshness of the dynamic flow to the cells but there was no evidence to support this. The mineralization results usually follow a similar trend with the cell number [183] but this was not seen in the results, where the dynamic condition with a higher cell proliferation was on a par with the static condition or lower. This might be because the cells under perfusion flow were in the phase of proliferation and had not begun to differentiate or accumulate ECM matrix. In similar terms, it was reported that lower mineralization area was observed in bioreactor cultured cells which had the highest levels of proliferation [138]. Also, the high 14-day mineralization result by Rodrigues et al. (2012) for hASCs at 0.1 mL/min/scaffold flow rate demanded OM, whereas in MM there was no difference between dynamic and static condition [35].

It should also be noted that the mineralization results were obtained at different flow rates and with different structures; flow rate of 0.25 mL/min/scaffold with the regular PLCL-β-TCP scaffolds and 0.50 mL/min/scaffold for the channel scaffolds. Due to shortage of scaffolds, the mineralization results were obtained from a limited number of samples;

only 1 static sample was available for channel scaffolds. Because of the asymmetric experiment design, the results were not fully comparable.

Mineral deposition of bone tissue is linked to extracellular pH and a slightly alkaline pH environment is required for mineralization to proceed [187]. The alkaline pH occurs during later bone tissue healing phases with the gradual increase of calcium content in the tissue matrix. The measured pH value of the dynamic condition was slightly more alkaline at pH 8.8 compared to 8.5 of the static control condition. However, this increase was not sufficient to rescue the calcium containing mineral deposition. The cause of the raise in the pH value in the flow system remained undetermined. Therefore, it can be concluded that no significant mineralized ECM was formed in the flow perfusion culture and there were no results showing late osteogenic differentiation of the hASCs in the structure comparison.

Overall cell culture results

The most potential cell culture results were obtained with the channel scaffolds with 1 week of static culture followed by 1 week of dynamic culture based on the results for cell viability and distribution (Figure 17). However, there were no significant results of hASC osteogenic differentiation in any of the tested conditions or structures. This was against our initial assumption and published results where perfusion flow bioreactor has been shown to induce hBMSC and hASC osteogenic differentiation even in MM [15; 16; 18; 37; 162]. Therefore, some other factors in the experiment design should be discussed, such as scaffold material and structure, flow rate, flow profile, fluid shear stress, and combined chemical stimulus to fully utilize perfusion flow for hASC osteogenic differentiation.

5.4.4 Scaffold material and structure

Scaffold material

As biomaterials, PLA and PCL are hydrophobic, whereas bioactive β-TCP increased the hydrophilicity of the composite biomaterial, according to the results published by Ahola et al. (2012) [87]. In a study by Marino et al. (2010) with β-TCP scaffolds, MM supported only weak osteogenic differentiation of hASCs, but in comparison, OM supported a higher qALP result [78]. Published data indicates that polymer composite scaffold material starts to release β-TCP already at 2 weeks compared to the 10-weeks required for the polymer component which means that the calcium component has been exposed and available to cells [87]. However, the exposure might have been too brief or available only in parts of the cell adhesion surface. In addition, hASCs remained rounded with little adhesion surface under the flow which might explain the negligeable impact of β-TCP. Higher percentage of β-TCP granules with rougher and more active surface might prove beneficial for increased osteogenesis in the composite scaffolds. The granules might have been embedded deeper in the material which made it harder to become exposed or

available for cells on the scaffold surface. Polymer encapsulated β-TCP granules might have been available for cells only in the manually cut surfaces. The partly crushed β-TCP might have been exposed in the scaffold top and bottom surfaces in addition to the channel structures where the exposed bioactive β-TCP might have attracted hASCs to adhere.

Scaffold structure

The supercritical CO_2 processing method resulted in a highly porous albeit irregular scaffold structure and the irregular pore structure might have prevented effective fluid flow interior of the scaffold. Also, in some instances, the irregular scaffold structure might have compromised even hASC distribution visible in the scaffold crosscut images. For comparison, homogenous cell distribution in perfusion culture was achieved for critical size bone grafts in a recent study by Kleinhans et al. (2015) [163]. Therefore, higher repeatability of the scaffold interior structure might prevent these issues. In order to apply efficiently mechanical stimuli with perfusion flow in porous scaffolds, the control of scaffold interior geometry with pore size and pore interconnectivity is crucial. The combined effects of flow and scaffold architecture have been shown as necessary parameters to optimize a perfusion flow system for osteogenic differentiation and signal expression. [32; 88; 188]. In this study, the PLCL-β-TCP composite scaffolds had pore sizes in the range of 300–500 μm pore size and 58 % porosity, determined previously with micro-CT imaging. Similar cell density was used in a study by Boschetti et al. (2006), where hASCs were induced towards osteogenic lineage on β-TCP scaffolds of similar dimensions with 200–500 μm pore size but with 82 % porosity [8]. Comparing these, the difference in pore size is small whereas the porosity differs considerably, and this might have lead to the different results.

The CT imaging could offer a more accurate view of the scaffold structure and help predict fluid flow behavior [189]. Micro-CT analysis is normally based on isotropic slices and random pore size and pore distribution might have hindered accurate analysis of heterogeneous scaffold morphology. Therefore, construct porosity might have been poorly defined. In addition, micro-CT resolution is approximately 20 μm and any pore walls thinner than this might have been left undetected. For more repeatable cell culture results under flow perfusion, a standardized scaffold architecture fabricated with additive manufacture methods, for example, might be an efficient structure to overcome these design limitations [190].

The fluid flow might have been suboptimal for efficient hASC stimulation besides the structural irregularity of the PLCL-β-TCP composite scaffolds, also because the porous structure might have been squeezed closed to fluid flow when the wetted and expanded cell seeded scaffolds were tightly fitted to the holder plate holes. Further permeability studies to determine fluid flow through interconnected pores when subjected to pressure might help elucidate the issue in more detail [189; 191; 192].

5.4.5 Flow rate

The flow rate of 0.5 mL/min/scaffold might have been relatively harsh on hASCs, since osteoblasts *in vivo* experience flow rates in the range of 0.008 mL/min [32]. Osteoblastic cell viability and osteogenic gene expression of RUNX2, OC and ALP was maintained by a flow rate of 0.01 mL/min, whereas a flow rate of 1 mL/min caused massive cell necrosis [151].

Similarly to our results, in a study by Baumgartner et al. (2015), no difference was seen in cell distribution when hASCs were cultured under 0.3 or 0.5 mL/min/scaffold perfusion flow in MM for 9 days in PLGA-amorphous calcium phosphate scaffolds [37]. Further, osteoblasts have been shown to be affected by stepwise alterations of fluid shear stress [193].

There might be threshold values of flow rates that efficiently trigger cell responses but functional flow rates have not been clearly determined, since for hBMSCs flow rates as diverse as 0.1 mL/min and 3 mL/min have resulted in cell proliferation and osteogenic differentiation [33; 36]. On the contrary, according to other research results, it is rather the level of shear stress that determines bone formation, and not the flow rate [20]. However, the scaffold material and structure should be considered together with the flow rate because their interaction determines the forces experienced by the cells.

5.4.6 Flow profile

The applied continuous flow of culture media might be reconsidered. A pulsatile flow profile has been reported to improve cell adhesion and osteogenic differentiation [136; 194], and to induce early osteogenic differentiation of rat BMSCs compared to continuous perfusion [195]. In previously published study, dynamically alternating shear stress has been shown to induce hASC osteogenesis in pulsatile perfusion with OM [34]. In a study by Filipowska et al. (2016), a single short perfusion pulse was found sufficient to stimulate ostegenic differentiation of hBMSCs in porous scaffolds [196]. The results by Bölgen et al. (2008) also showed the importance of breaks in dynamic stimulation; the perfusion and compression regime was applied for 1 h per day and the cells recovered and secreted ECM during the rest period [197]. The pulsed flow profile retains the cell secreted factors in the microenvironment of the adhered cells. However, in a study by Kreke et al. (2008), both steady and pulsed perfusion profiles were found to activate mechanotransduction cell signaling pathways, the effect of which was visible only after the cells were allowed to differentiate in static culture following perfusion flow. [198]

The flow profile might prove to be crucial, because Correia et al. (2013) applied succesfully a flow perfusion bioreactor to stimulate strong hASC mineral deposition in OM with an alternating flow profile for initial 2 weeks of steady flow followed by 3 weeks of pulsatile flow. The results showed hASC gene expression of OPN increased, and strong immunostaining result of osteogenic proteins COL1, OPN, OC and BSP as well as micro-

CT verified strong mineralization of ECM. [34] These results indicated that while steady flow and chemical stimulus of OM sensitized hASCs to pulsatile flow, it was in fact the pulsatile pattern that enhanced mineralization because cell mechanosensitivity becomes saturated under continuous loading. In bone tissue, resting periods between mechanical stimulation periods allow desensitized bone cells to regain mechanosensitivity [132; 199]. Indeed, intermittent fluid flow enhances greater cell stimulation with respect to continuous low flow rate and, subsequently, the alternation of short term exposure combined with long term exposure upregulated osteogenic differentiation with respect to static culture [151; 200; 201]. The duration of the resting period has been suggested as a minimum of 8 h, and for hASCs, a 4-h stimulation followed by a 20-h rest has been tested for osteogenic differentiation [202; 203]. Still, hASCs needed OM to become sensitive to mechanical stimulation [77]. Short perfusion of very high flow of 2.5 mL/min promoted hBMSC osteogenesis of cells already committed to osteogenic lineage in a recent study by Filipowska et al. (2016) [196]. This indicates that stem cells need to be committed to osteogenic lineage before subjected to perfusion stimulation.

5.4.7 Fluid shear stress

An added pressure sensor would help determine the nature of mechanical stress that the cells endure in the bioreactor. The nature of applied pressure might prove a key concept to direct hASC differentiation towards osteogenic path. Research results have reported osteoblasts subjected to shear stresses in the region of 0.8–3.0 Pa *in vivo*. [204].

Interestingly, fluid shear might not regulate vibration induced proliferation and mineralization, and instead, cytoskeletal remodeling activity may play a more significant role in MSC mechanosensitivity. According to the reported results [81; 205], greatly different levels of acceleration, frequency, and fluid shear can result in similar MSC responses, perhaps suggesting that yet to be identified mechanism by which cells sense oscillations is only indirectly related to the mechanical cues considered here.

The modelling of fluid dynamics would help to evaluate the distribution of shear stress of fluid perfusion for the cells growing inside and on the periphery porous scaffold [60; 206]. Acosta et al. (2013) used a similar porous PLLA structure under perfusion flow and according to their model, there was higher fluid pressure and shear stress on the scaffold top surface [189]. However, computational modelling has its limits and additional experimental testing is required because it is nearly impossible to measure shear stress distribution inside microstructures.

5.4.8 Chemical stimulus

The perfusion flow bioreactor with the supercritical CO_2 fabricated PLCL-β-TCP scaffolds did not support hASC osteogenic differentiation with the selected parameters in the absence of added chemical factors. On this topic, Tirkkonen et al. (2011) showed that the hASCs require chemical induction to become sensitive to mechanical stimulus and to

be able to initiate osteogenic differentiation under vibration loading [77]. Similarly, Correia et al. (2013) reported that they perceived no significant differences in proliferation under perfusion flow and the hASCs needed initial chemical osteogenic induction to become sensitized to flow conditions [34]. This was confirmed by Ferroni et al. (2016) who reported that ASCs require OM for osteogenic initiation with mechanical stimulation [207]. The hASCs have been reported to require the combination of chemical and mechanical induction to differentiate also in other studies [53; 208].

According to a similar trend, Du et al. (2012) confirmed that combined chemical and mechanical stimulation upregulated hASC osteogenic differentiation further compared to chemical stimulation alone [208]. Also, the studies by Silva et al. (2014) and Fröhlich et al. (2010) demonstrated that hASCs showed only weak osteogenic differentiation in perfusion culture without chemical induction by OM [33; 36]. Furthermore, Prè et al. (2011) reported that while soluble factors are not essential, they nevertheless effectively enhance hASC osteogenic processes with low amplitude, high frequency vibration [209].

5.5 Flow perfusion bioreactor usability

The perfusion flow was partly inefficient in the cell culture experiments. The bioreactor chamber was only half filled with circulating media due to air accumulation into the system, possibly because of the mechanism of action of the peristaltic pump. The bioreactor system usability might benefit from the installation of a vent to help remove any accumulated gas inside the reactor chamber. The reactor circuit was assembled in a manner that might have caused underpressure in the upper chamber and the fluid was sucked through the scaffolds rather than perfused directly through the structure from the top towards bottom. An alternative assembling order that has been used in other studies (Figure 9) present the culture circuit assembled in a manner that placed the bioreactor chamber immediately after the peristaltic pump in the direction of the fluid flow, and where the medium reservoir is placed after the reactor chamber. This culture circuit assembling order pumps circulating fluid directly through the constructs. On the contrary, in this study, the medium reservoir was placed before the bioreactor chamber (Figure 15;16) to prevent disadvantageous cooling of media before reaching the cells in the reactor chamber.

The amount of cell culture medium circulating in the culture circuit was a moderate 75 mL compared to other reported volumes ranging between 100–210 mL, for a similar number of constructs [25; 35], and thus cost efficient, since the cell culture reagents constitute a considerable part of the running expenses. The cell culture medium turned opaque after a week of bioreactor culture, possibly due to protein residues precipitating under shear stress with the action of the peristaltic pump. However, this is a known issue with bioreactor cell culture and remains to be solved. Importantly, there were no microbial contaminations detected during these experiments. This was contrary to previously reported high contamination risk associated with bioreactor cell culture [124]. This proves

that the novel bioreactor system was able to retain aseptic conditions inside the closed culture circuit.

Initially, during the preliminary cell culture experiments, leakage of culture media was an issue with the smaller 0.8-mm diameter silicone pump hose due to the high 45 rpm pumping speed that wore the pump hose during 2-week experiments. This is a known issue with peristaltic pump bioreactor systems and the pump hose is a wearable part. The leakage issue was solved by swithing to a larger 1.7-mm diameter silicone pump hose that produced the same flow rate with a considerably lower pumping speed.

The bioreactor materials and parts endured multiple cycles of use, and only the silicone hoses were used once. The parts of the reactor chamber were washed and autoclaved at least 9 times during the experiments. Contrary to single-use bioreactor accessories, the novel bioreactor creates less waste because the parts are reusable. The design is streamlined and durable because there are no complicated electronics in the culture circuit. The custom-designed perfusion bioreactor is a modular system, offering high throughput scale-up opportunities and efficiency for treatment of a large number of scaffolds at a single loading.

The system is quick to assemble or disassemble, thus simplifying time consuming cell culture processes. It is portable, compact and lightweight for added usability. The multi-hole property of the holder plates makes the bioreactor system versatile and efficient with the expandable loading capacity of several scaffolds at a single loading. Compared to, for example, currently available commercial single specimen bioreactor chambers and their less practical multichamber assembly (Figure 10;11), the proposed new flow perfusion bioreactor prototype is more simple to operate.

5.6 Future perspectives

The more specific mechanical stimuli conditions that support hASC commitment towards osteogenic lineage could be researched further. Better characterization of the flow patterns and fluid dynamics within the flow perfusion bioreactor is needed to better understand the relationship between fluid shear and stem cell differentiation [144].

Application of defined flow rates can produce greatly different shear stresses acting on the cells depending on the scaffold microarchitecture. However, the complex non-regular structure of the supercritical CO_2 fabricated scaffolds might not allow accurate evaluation or even distribution of fluid in a repeatable manner, and the modelling results might be valid only for that specific specimen. The lack of a reproducible scaffold architecture might render it difficult to predict results of any experimental study. An optimized and highly porous structure with interconnected pores could intensify the effect of the fluid flow interior the construct for improved hASC stimulation.

Identifying the different cellular mechanotransduction events might shed more light to the molecular switches and cell signaling events involved in cellular mechanical sensing [57; 132]. Physical sensors would provide a noninvasive tool to monitor, control and collect data from the bioreactor environment [210]. For future applications of the perfusion flow bioreactor, the system design and especially fluid parameters need careful re-evaluation in order to optimize the functionality of the system for hASC osteogenic differentiation.

6 CONCLUSIONS

The main objective of this work was to test the applicability of the new flow perfusion bioreactor prototype for aseptic *in vitro* cell culture. In addition, another objective was to establish new osteogenic differentiation protocol for the hASCs with perfusion flow in the novel osteoconductive supercritical CO_2 processed PLCL-β-TCP scaffolds without added chemical stimulus.

The hASC viability, adhesion, distribution, and osteogenic differentiation in the PLCL-β-TCP polymer composite scaffolds at 2 different perfusion flow rates and 2 different scaffold structures was studied. Overall, in all the dynamic conditions, the hASCs showed a tendency to form dense cell aggregates and adapted a tightly rounded morphology, and loosely adhered to surface. According to the results, the perfusion flow maintained sufficiently cell viability in supercritical CO_2 processed PLCL-β-TCP scaffolds, although there were few necrotic cells visible in the scaffold crosscut plane which indicated insufficient fluid flow and mass transport due to irregularity of structure or fluid flow malfunction due to air accumulation. Overall, PLCL-β-TCP scaffolds supported hASC survival and the dynamic condition promoted round hASC morphology.

Most importantly, a greater cell number was gained in all dynamic conditions compared to the static controls. However, the results were not significantly higher and there was considerably less ECM accumulation in the form of total collagen content or ECM mineralization detected in the samples cultured under continuous perfusion flow compared to the static controls in all the experiments.

These results indicated that osteogenic soluble factors might be needed to support the hASC commitment towards osteogenic lineage as the structure or the fluid flow alone was not sufficient to promote hASC osteogenesis. Therefore, the optimal perfusion stimulation parameters to support hASC osteogenic differentiation in the novel supercritical CO_2 processed PLCL-β-TCP scaffolds remain to be defined (Table 6). In summary, the perfusion flow bioreactor prototype was nevertheless suitable for aseptic cell culture, easy to operate, possessed simple design and efficient loading capacity for multiple samples and, therefore, potential for further development.

Table 6. *Suggestions for future improvements of the flow perfusion bioreactor system to support human adipose stem cell (hASC) osteogenic differentiation.*

Issue	**Solutions**
Round hASC morphology	Optimized flow rate and profile that allows elongated hASC morphology
Unhomogeneous cell density under flow perfusion	More repeatable and functional scaffold structure needed
Lack of hASC osteogenic markers	More cell matrix growth with rest periods
	Initial chemical induction needed to sensitize hASCs for mechanical stimulus
	Effects of system parameters on cell proliferation and differentiation need further research

REFERENCES

[1] Q. Fu, E. Saiz, M.N. Rahaman, A.P. Tomsia, Bioactive glass scaffolds for bone tissue engineering: state of the art and future perspectives, Mater.Sci.Eng.C.Mater.Biol.Appl., Vol. 31, No. 7, 2011, pp. 1245-1256.

[2] A. Chatterjea, G. Meijer, C. van Blitterswijk, J. de Boer, Clinical application of human mesenchymal stromal cells for bone tissue engineering, Stem Cells Int., 2010, pp. 215625.

[3] J.E. Schroeder & R. Mosheiff, Tissue engineering approaches for bone repair: concepts and evidence, Injury, Vol. 42, No. 6, 2011, pp. 609-613.

[4] W.L. Grayson, B.A. Bunnell, E. Martin, T. Frazier, B.P. Hung, J.M. Gimble, Stromal cells and stem cells in clinical bone regeneration, Nat.Rev.Endocrinol., Vol. 11, No. 3, 2015, pp. 140-150.

[5] R. Langer & J.P. Vacanti, Tissue engineering, Science, Vol. 260, No. 5110, 1993, pp. 920-926.

[6] R. Langer, Tissue engineering, Mol.Ther., Vol. 1, No. 1, 2000, pp. 12-15.

[7] P. Thevenot, A. Nair, J. Dey, J. Yang, L. Tang, Method to analyze three-dimensional cell distribution and infiltration in degradable scaffolds, Tissue Eng.Part C.Methods, Vol. 14, No. 4, 2008, pp. 319-331.

[8] F. Boschetti, M.T. Raimondi, F. Migliavacca, G. Dubini, Prediction of the micro-fluid dynamic environment imposed to three-dimensional engineered cell systems in bioreactors, J.Biomech., Vol. 39, No. 3, 2006, pp. 418-425.

[9] Y. Reinwald, R.K. Johal, A.M. Ghaemmaghami, F.R.A.J. Rose, S.M. Howdle, K.M. Shakesheff, Interconnectivity and permeability of supercritical fluid-foamed scaffolds and the effect of their structural properties on cell distribution, Polymer, Vol. 55, No. 1, 2014, pp. 435-444.

[10] B. Lindroos, R. Suuronen, S. Miettinen, The potential of adipose stem cells in regenerative medicine, Stem Cell.Rev., Vol. 7, No. 2, 2011, pp. 269-291.

[11] A. Kraus, C. Woon, S. Raghavan, K. Megerle, H. Pham, J. Chang, Co-culture of human adipose-derived stem cells with tenocytes increases proliferation and induces

differentiation into a tenogenic lineage, Plast.Reconstr.Surg., Vol. 132, No. 5, 2013, pp. 754e-66e.

[12] V. Vindigni, C. Tonello, L. Lancerotto, G. Abatangelo, R. Cortivo, B. Zavan, F. Bassetto, Preliminary report of in vitro reconstruction of a vascularized tendonlike structure: a novel application for adipose-derived stem cells, Ann.Plast.Surg., Vol. 71, No. 6, 2013, pp. 664-670.

[13] J.A. Vina, M. El-Alami, J. Gambini, C. Borras, J. Vina, M.A. Penarrocha, Application of mesenchymal stem cells in bone regenerative procedures in oral implantology. A literature review, J.Clin.Exp.Dent., Vol. 6, No. 1, 2014, pp. e60-e65.

[14] K. Mesimaki, B. Lindroos, J. Tornwall, J. Mauno, C. Lindqvist, R. Kontio, S. Miettinen, R. Suuronen, Novel maxillary reconstruction with ectopic bone formation by GMP adipose stem cells, Int.J.Oral Maxillofac.Surg., Vol. 38, No. 3, 2009, pp. 201-209.

[15] L. Bjerre, C.E. Bunger, M. Kassem, T. Mygind, Flow perfusion culture of human mesenchymal stem cells on silicate-substituted tricalcium phosphate scaffolds, Biomaterials, Vol. 29, No. 17, 2008, pp. 2616-2627.

[16] L. Bjerre, C. Bunger, A. Baatrup, M. Kassem, T. Mygind, Flow perfusion culture of human mesenchymal stem cells on coralline hydroxyapatite scaffolds with various pore sizes, J.Biomed.Mater.Res.A., Vol. 97, No. 3, 2011, pp. 251-263.

[17] F. Zhao, R. Chella, T. Ma, Effects of shear stress on 3-D human mesenchymal stem cell construct development in a perfusion bioreactor system: Experiments and hydrodynamic modeling, Biotechnol.Bioeng., Vol. 96, No. 3, 2007, pp. 584-595.

[18] F. Zhao, W.L. Grayson, T. Ma, A. Irsigler, Perfusion affects the tissue developmental patterns of human mesenchymal stem cells in 3D scaffolds, J.Cell.Physiol., Vol. 219, No. 2, 2009, pp. 421-429.

[19] J. Kim & T. Ma, Bioreactor strategy in bone tissue engineering: pre-culture and osteogenic differentiation under two flow configurations, Tissue Eng.Part A., Vol. 18, No. 21-22, 2012, pp. 2354-2364.

[20] D. Li, T. Tang, J. Lu, K. Dai, Effects of flow shear stress and mass transport on the construction of a large-scale tissue-engineered bone in a perfusion bioreactor, Tissue Eng.Part A., Vol. 15, No. 10, 2009, pp. 2773-2783.

[21] J. Yang, C. Cao, W. Wang, X. Tong, D. Shi, F. Wu, Q. Zheng, C. Guo, Z. Pan, C. Gao, J. Wang, Proliferation and osteogenesis of immortalized bone marrow-derived

mesenchymal stem cells in porous polylactic glycolic acid scaffolds under perfusion culture, J.Biomed.Mater.Res.A., Vol. 92, No. 3, 2010, pp. 817-829.

[22] C. Kleinhans, R.R. Mohan, G. Vacun, T. Schwarz, B. Haller, Y. Sun, A. Kahlig, P. Kluger, A. Finne-Wistrand, H. Walles, J. Hansmann, A perfusion bioreactor system efficiently generates cell-loaded bone substitute materials for addressing critical size bone defects, Biotechnol.J., Vol. 10, No. 11, 2015, pp. 1727-1738.

[23] G.N. Bancroft, V.I. Sikavitsas, A.G. Mikos, Design of a flow perfusion bioreactor system for bone tissue-engineering applications, Tissue Eng., Vol. 9, No. 3, 2003, pp. 549-554.

[24] R.A. Thibault, A.G. Mikos, F.K. Kasper, Protein and mineral composition of osteogenic extracellular matrix constructs generated with a flow perfusion bioreactor, Biomacromolecules, Vol. 12, No. 12, 2011, pp. 4204-4212.

[25] M.E. Gomes, V.I. Sikavitsas, E. Behravesh, R.L. Reis, A.G. Mikos, Effect of flow perfusion on the osteogenic differentiation of bone marrow stromal cells cultured on starch-based three-dimensional scaffolds, J.Biomed.Mater.Res.A., Vol. 67, No. 1, 2003, pp. 87-95.

[26] M.E. Gomes, H.L. Holtorf, R.L. Reis, A.G. Mikos, Influence of the porosity of starch-based fiber mesh scaffolds on the proliferation and osteogenic differentiation of bone marrow stromal cells cultured in a flow perfusion bioreactor, Tissue Eng., Vol. 12, No. 4, 2006, pp. 801-809.

[27] H.L. Holtorf, J.A. Jansen, A.G. Mikos, Ectopic bone formation in rat marrow stromal cell/titanium fiber mesh scaffold constructs: effect of initial cell phenotype, Biomaterials, Vol. 26, No. 31, 2005, pp. 6208-6216.

[28] H.L. Holtorf, J.A. Jansen, A.G. Mikos, Flow perfusion culture induces the osteoblastic differentiation of marrow stroma cell-scaffold constructs in the absence of dexamethasone, J.Biomed.Mater.Res.A., Vol. 72, No. 3, 2005, pp. 326-334.

[29] V.I. Sikavitsas, G.N. Bancroft, J.J. Lemoine, M.A. Liebschner, M. Dauner, A.G. Mikos, Flow perfusion enhances the calcified matrix deposition of marrow stromal cells in biodegradable nonwoven fiber mesh scaffolds, Ann.Biomed.Eng., Vol. 33, No. 1, 2005, pp. 63-70.

[30] V.I. Sikavitsas, G.N. Bancroft, H.L. Holtorf, J.A. Jansen, A.G. Mikos, Mineralized matrix deposition by marrow stromal osteoblasts in 3D perfusion culture increases with increasing fluid shear forces, Proc.Natl.Acad.Sci.U.S.A., Vol. 100, No. 25, 2003, pp. 14683-14688.

[31] M.J. Jaasma, N.A. Plunkett, F.J. O'Brien, Design and validation of a dynamic flow perfusion bioreactor for use with compliant tissue engineering scaffolds, J.Biotechnol., Vol. 133, No. 4, 2008, pp. 490-496.

[32] M. Bartnikowski, T.J. Klein, F.P. Melchels, M.A. Woodruff, Effects of scaffold architecture on mechanical characteristics and osteoblast response to static and perfusion bioreactor cultures, Biotechnol.Bioeng., Vol. 111, No. 7, 2014, pp. 1440-1451.

[33] A.R. Silva, A.C. Paula, T.M. Martins, A.M. Goes, M.M. Pereria, Synergistic effect between bioactive glass foam and a perfusion bioreactor on osteogenic differentiation of human adipose stem cells, J.Biomed.Mater.Res.A., Vol. 102, No. 3, 2014, pp. 818-827.

[34] C. Correia, S. Bhumiratana, R.A. Sousa, R.L. Reis, G. Vunjak-Novakovic, Sequential application of steady and pulsatile medium perfusion enhanced the formation of engineered bone, Tissue Eng.Part A., Vol. 19, No. 9-10, 2013, pp. 1244-1254.

[35] A.I. Rodrigues, M.E. Gomes, I.B. Leonor, R.L. Reis, Bioactive starch-based scaffolds and human adipose stem cells are a good combination for bone tissue engineering, Acta Biomater., Vol. 8, No. 10, 2012, pp. 3765-3776.

[36] M. Frohlich, W.L. Grayson, D. Marolt, J.M. Gimble, N. Kregar-Velikonja, G. Vunjak-Novakovic, Bone grafts engineered from human adipose-derived stem cells in perfusion bioreactor culture, Tissue Eng.Part A., Vol. 16, No. 1, 2010, pp. 179-189.

[37] W. Baumgartner, M. Welti, N. Hild, S.C. Hess, W.J. Stark, G.M. Burgisser, P. Giovanoli, J. Buschmann, Tissue mechanics of piled critical size biomimetic and biominerizable nanocomposites: Formation of bioreactor-induced stem cell gradients under perfusion and compression, J.Mech.Behav.Biomed.Mater., Vol. 47, 2015, pp. 124-134.

[38] S. Guven, A. Mehrkens, F. Saxer, D.J. Schaefer, R. Martinetti, I. Martin, A. Scherberich, Engineering of large osteogenic grafts with rapid engraftment capacity using mesenchymal and endothelial progenitors from human adipose tissue, Biomaterials, Vol. 32, No. 25, 2011, pp. 5801-5809.

[39] A. Scherberich, R. Galli, C. Jaquiery, J. Farhadi, I. Martin, Three-dimensional perfusion culture of human adipose tissue-derived endothelial and osteoblastic progenitors generates osteogenic constructs with intrinsic vascularization capacity, Stem Cells, Vol. 25, No. 7, 2007, pp. 1823-1829.

[40] R. Khanna-Jain, B. Mannerstrom, A. Vuorinen, G.K. Sandor, R. Suuronen, S. Miettinen, Osteogenic differentiation of human dental pulp stem cells on beta-tricalcium phosphate/poly (l-lactic acid/caprolactone) three-dimensional scaffolds, J.Tissue Eng., Vol. 3, No. 1, 2012, pp. 2041731412467998.

[41] P. Muller, U. Bulnheim, A. Diener, F. Luthen, M. Teller, E.D. Klinkenberg, H.G. Neumann, B. Nebe, A. Liebold, G. Steinhoff, J. Rychly, Calcium phosphate surfaces promote osteogenic differentiation of mesenchymal stem cells, J.Cell.Mol.Med., Vol. 12, No. 1, 2008, pp. 281-291.

[42] A. Larranaga, E. Diamanti, E. Rubio, T. Palomares, A. Alonso-Varona, P. Aldazabal, F.J. Martin, J.R. Sarasua, A study of the mechanical properties and cytocompatibility of lactide and caprolactone based scaffolds filled with inorganic bioactive particles, Mater.Sci.Eng.C.Mater.Biol.Appl., Vol. 42, 2014, pp. 451-460.

[43] A. Larranaga, A. Alonso-Varona, T. Palomares, E. Rubio-Azpeitia, P. Aldazabal, F.J. Martin, J.R. Sarasua, Effect of bioactive glass particles on osteogenic differentiation of adipose-derived mesenchymal stem cells seeded on lactide and caprolactone based scaffolds, J.Biomed.Mater.Res.A., Vol. 103, No. 12, 2015, pp. 3815-3824.

[44] Z. Cui, B. Nelson, Y. Peng, K. Li, S. Pilla, W.J. Li, L.S. Turng, C. Shen, Fabrication and characterization of injection molded poly (epsilon-caprolactone) and poly (epsilon-caprolactone)/hydroxyapatite scaffolds for tissue engineering, Mater.Sci.Eng.C.Mater.Biol.Appl., Vol. 32, No. 6, 2012, pp. 1674-1681.

[45] D.M. Choumerianou, H. Dimitriou, M. Kalmanti, Stem cells: promises versus limitations, Tissue Eng.Part B.Rev., Vol. 14, No. 1, 2008, pp. 53-60.

[46] J. Jensen, J. Hyllner, P. Bjorquist, Human embryonic stem cell technologies and drug discovery, J.Cell.Physiol., Vol. 219, No. 3, 2009, pp. 513-519.

[47] K. Takahashi & S. Yamanaka, Induction of pluripotent stem cells from mouse embryonic and adult fibroblast cultures by defined factors, Cell, Vol. 126, No. 4, 2006, pp. 663-676.

[48] M. Grskovic, A. Javaherian, B. Strulovici, G.Q. Daley, Induced pluripotent stem cells--opportunities for disease modelling and drug discovery, Nat.Rev.Drug Discov., Vol. 10, No. 12, 2011, pp. 915-929.

[49] M. Dominici, K. Le Blanc, I. Mueller, I. Slaper-Cortenbach, F. Marini, D. Krause, R. Deans, A. Keating, D. Prockop, E. Horwitz, Minimal criteria for defining

multipotent mesenchymal stromal cells. The International Society for Cellular Therapy position statement, Cytotherapy, Vol. 8, No. 4, 2006, pp. 315-317.

[50] P. Bourin, B.A. Bunnell, L. Casteilla, M. Dominici, A.J. Katz, K.L. March, H. Redl, J.P. Rubin, K. Yoshimura, J.M. Gimble, Stromal cells from the adipose tissue-derived stromal vascular fraction and culture expanded adipose tissue-derived stromal/stem cells: a joint statement of the International Federation for Adipose Therapeutics and Science (IFATS) and the International Society for Cellular Therapy (ISCT), Cytotherapy, Vol. 15, No. 6, 2013, pp. 641-648.

[51] P.A. Zuk, M. Zhu, H. Mizuno, J. Huang, J.W. Futrell, A.J. Katz, P. Benhaim, H.P. Lorenz, M.H. Hedrick, Multilineage cells from human adipose tissue: implications for cell-based therapies, Tissue Eng., Vol. 7, No. 2, 2001, pp. 211-228.

[52] A. Park, M.V. Hogan, G.S. Kesturu, R. James, G. Balian, A.B. Chhabra, Adipose-derived mesenchymal stem cells treated with growth differentiation factor-5 express tendon-specific markers, Tissue Eng.Part A., Vol. 16, No. 9, 2010, pp. 2941-2951.

[53] K. Vuornos, M. Bjorninen, E. Talvitie, K. Paakinaho, M. Kellomaki, H. Huhtala, S. Miettinen, R. Seppanen-Kaijansinkko, S. Haimi, Human Adipose Stem Cells Differentiated on Braided Polylactide Scaffolds Is a Potential Approach for Tendon Tissue Engineering, Tissue Eng.Part A., Vol. 22, No. 5-6, 2016, pp. 513-523.

[54] T. Thesleff, K. Lehtimaki, T. Niskakangas, B. Mannerstrom, S. Miettinen, R. Suuronen, J. Ohman, Cranioplasty with adipose-derived stem cells and biomaterial: a novel method for cranial reconstruction, Neurosurgery, Vol. 68, No. 6, 2011, pp. 1535-1540.

[55] L.A. Meza-Zepeda, A. Noer, J.A. Dahl, F. Micci, O. Myklebost, P. Collas, High-resolution analysis of genetic stability of human adipose tissue stem cells cultured to senescence, J.Cell.Mol.Med., Vol. 12, No. 2, 2008, pp. 553-563.

[56] G.K. Sandor, V.J. Tuovinen, J. Wolff, M. Patrikoski, J. Jokinen, E. Nieminen, B. Mannerstrom, O.P. Lappalainen, R. Seppanen, S. Miettinen, Adipose stem cell tissue-engineered construct used to treat large anterior mandibular defect: a case report and review of the clinical application of good manufacturing practice-level adipose stem cells for bone regeneration, J.Oral Maxillofac.Surg., Vol. 71, No. 5, 2013, pp. 938-950.

[57] N. Plunkett & F.J. O'Brien, IV.3. Bioreactors in tissue engineering, Stud.Health Technol.Inform., Vol. 152, 2010, pp. 214-230.

[58] R. Narayan, ed., Biomedical materials, Springer, New York, NY, USA, 2009, 566 p.

[59] M.M. Stevens, Biomaterials for bone tissue engineering, Materials Today, Vol. 11, No. 5, 2008, pp. 18-25.

[60] A.C. Allori, E.H. Davidson, D.D. Reformat, A.M. Sailon, J. Freeman, A. Vaughan, D. Wootton, E. Clark, J.L. Ricci, S.M. Warren, Design and validation of a dynamic cell-culture system for bone biology research and exogenous tissue-engineering applications, J.Tissue Eng.Regen.Med., Vol. 10, No. 10, 2016, pp. E327-E336.

[61] E.H. Davidson, D.D. Reformat, A. Allori, O. Canizares, I. Janelle Wagner, P.B. Saadeh, S.M. Warren, Flow perfusion maintains ex vivo bone viability: a novel model for bone biology research, J.Tissue Eng.Regen.Med., Vol. 6, No. 10, 2012, pp. 769-776.

[62] S.P. Fritton & S. Weinbaum, Fluid and Solute Transport in Bone: Flow-Induced Mechanotransduction, Annu.Rev.Fluid Mech., Vol. 41, 2009, pp. 347-374.

[63] C. Price, X. Zhou, W. Li, L. Wang, Real-time measurement of solute transport within the lacunar-canalicular system of mechanically loaded bone: direct evidence for load-induced fluid flow, J.Bone Miner.Res., Vol. 26, No. 2, 2011, pp. 277-285.

[64] J. Klein-Nulend, R.G. Bacabac, A.D. Bakker, Mechanical loading and how it affects bone cells: the role of the osteocyte cytoskeleton in maintaining our skeleton, Eur.Cell.Mater., Vol. 24, 2012, pp. 278-291.

[65] F. Long, Building strong bones: molecular regulation of the osteoblast lineage, Nat.Rev.Mol.Cell Biol., Vol. 13, No. 1, 2011, pp. 27-38.

[66] B.K. Hall, Bones and Cartilage: Developmental and Evolutionary Skeletal Biology 1, Elsevier Academic Press, San Diego, CA, USA, 2005, 760 p.

[67] J.B. Lian, G.S. Stein, A.J. van Wijnen, J.L. Stein, M.Q. Hassan, T. Gaur, Y. Zhang, MicroRNA control of bone formation and homeostasis, Nat.Rev.Endocrinol., Vol. 8, No. 4, 2012, pp. 212-227.

[68] A. Schaffler & C. Buchler, Concise review: adipose tissue-derived stromal cells--basic and clinical implications for novel cell-based therapies, Stem Cells, Vol. 25, No. 4, 2007, pp. 818-827.

[69] H.V. Desai, I.S. Voruganti, C. Jayasuriya, Q. Chen, E.M. Darling, Live-cell, temporal gene expression analysis of osteogenic differentiation in adipose-derived stem cells, Tissue Eng.Part A., Vol. 20, No. 5-6, 2014, pp. 899-907.

[70] H. Orimo, The mechanism of mineralization and the role of alkaline phosphatase in health and disease, J.Nippon Med.Sch., Vol. 77, No. 1, 2010, pp. 4-12.

[71] J.B. Lian & G.S. Stein, Development of the osteoblast phenotype: molecular mechanisms mediating osteoblast growth and differentiation, Iowa Orthop.J., Vol. 15, 1995, pp. 118-140.

[72] L. Kyllonen, S. Haimi, B. Mannerstrom, H. Huhtala, K.M. Rajala, H. Skottman, G.K. Sandor, S. Miettinen, Effects of different serum conditions on osteogenic differentiation of human adipose stem cells in vitro, Stem Cell.Res.Ther., Vol. 4, No. 1, 2013, pp. 17.

[73] K.R. Garrison, I. Shemilt, S. Donell, J.J. Ryder, M. Mugford, I. Harvey, F. Song, V. Alt, Bone morphogenetic protein (BMP) for fracture healing in adults, Cochrane Database Syst.Rev., Vol. (6):CD006950. doi, No. 6, 2010, pp. CD006950.

[74] K.R. Garrison, S. Donell, J. Ryder, I. Shemilt, M. Mugford, I. Harvey, F. Song, Clinical effectiveness and cost-effectiveness of bone morphogenetic proteins in the non-healing of fractures and spinal fusion: a systematic review, Health Technol.Assess., Vol. 11, No. 30, 2007, pp. 1-150, iii-iv.

[75] P. Zuk, Y.F. Chou, F. Mussano, P. Benhaim, B.M. Wu, Adipose-derived stem cells and BMP2: part 2. BMP2 may not influence the osteogenic fate of human adipose-derived stem cells, Connect.Tissue Res., Vol. 52, No. 2, 2011, pp. 119-132.

[76] J. Pelto, M. Bjorninen, A. Palli, E. Talvitie, J. Hyttinen, B. Mannerstrom, R. Suuronen Seppanen, M. Kellomaki, S. Miettinen, S. Haimi, Novel polypyrrole-coated polylactide scaffolds enhance adipose stem cell proliferation and early osteogenic differentiation, Tissue Eng.Part A., Vol. 19, No. 7-8, 2013, pp. 882-892.

[77] L. Tirkkonen, H. Halonen, J. Hyttinen, H. Kuokkanen, H. Sievanen, A.M. Koivisto, B. Mannerstrom, G.K. Sandor, R. Suuronen, S. Miettinen, S. Haimi, The effects of vibration loading on adipose stem cell number, viability and differentiation towards bone-forming cells, J.R.Soc.Interface, Vol. 8, No. 65, 2011, pp. 1736-1747.

[78] G. Marino, F. Rosso, G. Cafiero, C. Tortora, M. Moraci, M. Barbarisi, A. Barbarisi, Beta-tricalcium phosphate 3D scaffold promote alone osteogenic differentiation of human adipose stem cells: in vitro study, J.Mater.Sci.Mater.Med., Vol. 21, No. 1, 2010, pp. 353-363.

[79] A.S. Zanetti, G.T. McCandless, J.Y. Chan, J.M. Gimble, D.J. Hayes, In vitro human adipose-derived stromal/stem cells osteogenesis in akermanite:poly-epsilon-caprolactone scaffolds, J.Biomater.Appl., Vol. 28, No. 7, 2014, pp. 998-1007.

[80] B. Altmann, A. Lochner, M. Swain, R.J. Kohal, S. Giselbrecht, E. Gottwald, T. Steinberg, P. Tomakidi, Differences in morphogenesis of 3D cultured primary human osteoblasts under static and microfluidic growth conditions, Biomaterials, Vol. 35, No. 10, 2014, pp. 3208-3219.

[81] R.J. McCoy & F.J. O'Brien, Influence of shear stress in perfusion bioreactor cultures for the development of three-dimensional bone tissue constructs: a review, Tissue Eng.Part B.Rev., Vol. 16, No. 6, 2010, pp. 587-601.

[82] C. van Blitterswijk, Tissue engineering 1, Academic Press, Amsterdam, the Netherlands, 2008, 740 p.

[83] A.M. Barradas, V. Monticone, M. Hulsman, C. Danoux, H. Fernandes, Z. Tahmasebi Birgani, F. Barrere-de Groot, H. Yuan, M. Reinders, P. Habibovic, C. van Blitterswijk, J. de Boer, Molecular mechanisms of biomaterial-driven osteogenic differentiation in human mesenchymal stromal cells, Integr.Biol.(Camb), Vol. 5, No. 7, 2013, pp. 920-931.

[84] P.P. Vergroesen, R.J. Kroeze, M.N. Helder, T.H. Smit, The use of poly(L-lactide-co-caprolactone) as a scaffold for adipose stem cells in bone tissue engineering: application in a spinal fusion model, Macromol.Biosci., Vol. 11, No. 6, 2011, pp. 722-730.

[85] S.H. Kim, Y. Jung, S.H. Kim, A biocompatible tissue scaffold produced by supercritical fluid processing for cartilage tissue engineering, Tissue Eng.Part C.Methods, Vol. 19, No. 3, 2013, pp. 181-188.

[86] L. Cui, B. Liu, G. Liu, W. Zhang, L. Cen, J. Sun, S. Yin, W. Liu, Y. Cao, Repair of cranial bone defects with adipose derived stem cells and coral scaffold in a canine model, Biomaterials, Vol. 28, No. 36, 2007, pp. 5477-5486.

[87] N. Ahola, M. Veiranto, J. Rich, A. Efimov, M. Hannula, J. Seppala, M. Kellomaki, Hydrolytic degradation of composites of poly(L-lactide-co-E-caprolactone) 70/30 and beta-tricalcium phosphate, J.Biomater.Appl., 2012,

[88] V. Karageorgiou & D. Kaplan, Porosity of 3D biomaterial scaffolds and osteogenesis, Biomaterials, Vol. 26, No. 27, 2005, pp. 5474-5491.

[89] J.J. Alm, J.P. Frantzen, N. Moritz, P. Lankinen, M. Tukiainen, M. Kellomaki, H.T. Aro, In vivo testing of a biodegradable woven fabric made of bioactive glass fibers and PLGA80--a pilot study in the rabbit, J.Biomed.Mater.Res.B.Appl.Biomater., Vol. 93, No. 2, 2010, pp. 573-580.

[90] C. Weinand, J.W. Xu, G.M. Peretti, L.J. Bonassar, T.J. Gill, Conditions affecting cell seeding onto three-dimensional scaffolds for cellular-based biodegradable implants, J.Biomed.Mater.Res.B.Appl.Biomater., Vol. 91, No. 1, 2009, pp. 80-87.

[91] W.L. Murphy, T.C. McDevitt, A.J. Engler, Materials as stem cell regulators, Nat.Mater., Vol. 13, No. 6, 2014, pp. 547-557.

[92] J.R. Jones, New trends in bioactive scaffolds: The importance of nanostructure, Journal of the European Ceramic Society, Vol. 29, No. 7, 2009, pp. 1275-1281.

[93] J. Li, X. Liu, B. Zuo, L. Zhang, The Role of Bone Marrow Microenvironment in Governing the Balance between Osteoblastogenesis and Adipogenesis, Aging Dis., Vol. 7, No. 4, 2015, pp. 514-525.

[94] A. Trumbull, G. Subramanian, E. Yildirim-Ayan, Mechanoresponsive musculoskeletal tissue differentiation of adipose-derived stem cells, Biomed.Eng.Online, Vol. 15, 2016, pp. 43-016-0150-9.

[95] R.M. Rasal, A.V. Janorkar, D.E. Hirt, Poly(lactic acid) modifications, Progress in Polymer Science, Vol. 35, No. 3, 2010, pp. 338-356.

[96] L.S. Nair & C.T. Laurencin, Polymers as biomaterials for tissue engineering and controlled drug delivery, Adv.Biochem.Eng.Biotechnol., Vol. 102, 2006, pp. 47-90.

[97] D.W. Hutmacher, Scaffolds in tissue engineering bone and cartilage, Biomaterials, Vol. 21, No. 24, 2000, pp. 2529-2543.

[98] H. Yuan, H. Fernandes, P. Habibovic, J. de Boer, A.M. Barradas, A. de Ruiter, W.R. Walsh, C.A. van Blitterswijk, J.D. de Bruijn, Osteoinductive ceramics as a synthetic alternative to autologous bone grafting, Proc.Natl.Acad.Sci.U.S.A., Vol. 107, No. 31, 2010, pp. 13614-13619.

[99] A. Kolk, J. Handschel, W. Drescher, D. Rothamel, F. Kloss, M. Blessmann, M. Heiland, K.D. Wolff, R. Smeets, Current trends and future perspectives of bone substitute materials - from space holders to innovative biomaterials, J.Craniomaxillofac.Surg., Vol. 40, No. 8, 2012, pp. 706-718.

[100] J.M. Toth, H.S. An, T.H. Lim, Y. Ran, N.G. Weiss, W.R. Lundberg, R.M. Xu, K.L. Lynch, Evaluation of porous biphasic calcium phosphate ceramics for anterior cervical interbody fusion in a caprine model, Spine (Phila Pa.1976), Vol. 20, No. 20, 1995, pp. 2203-2210.

[101] J.X. Lu, B. Flautre, K. Anselme, P. Hardouin, A. Gallur, M. Descamps, B. Thierry, Role of interconnections in porous bioceramics on bone recolonization in vitro and in vivo, J.Mater.Sci.Mater.Med., Vol. 10, No. 2, 1999, pp. 111-120.

[102] DePuy Synthes. August 12, 2016, chronOS® bone graft substitute. [WWW]. Available, (accessed 15.08.2016): https://www.depuysynthes.com/hcp/biomaterials/products/qs/chronOS-bone-graft-subst-cmf.

[103] W.L. Murphy, T.C. McDevitt, A.J. Engler, Materials as stem cell regulators, Nat.Mater., Vol. 13, No. 6, 2014, pp. 547-557.

[104] A.J. Lasprilla, G.A. Martinez, B.H. Lunelli, A.L. Jardini, R.M. Filho, Poly-lactic acid synthesis for application in biomedical devices - a review, Biotechnol.Adv., Vol. 30, No. 1, 2012, pp. 321-328.

[105] G. Narayanan, V.N. Vernekar, E.L. Kuyinu, C.T. Laurencin, Poly (lactic acid)-based biomaterials for orthopaedic regenerative engineering, Adv.Drug Deliv.Rev., 2016.

[106] I. Izal, P. Aranda, P. Sanz-Ramos, P. Ripalda, G. Mora, F. Granero-Molto, H. Deplaine, J.L. Gomez-Ribelles, G.G. Ferrer, V. Acosta, I. Ochoa, J.M. Garcia-Aznar, E.J. Andreu, M. Monleon-Pradas, M. Doblare, F. Prosper, Culture of human bone marrow-derived mesenchymal stem cells on of poly(L-lactic acid) scaffolds: potential application for the tissue engineering of cartilage, Knee Surg.Sports Traumatol.Arthrosc., Vol. 21, No. 8, 2013, pp. 1737-1750.

[107] K. Vuornos, M. Bjorninen, E. Talvitie, K. Paakinaho, M. Kellomaki, H. Huhtala, S. Miettinen, R. Seppanen-Kaijansinkko, S. Haimi, Human Adipose Stem Cells Differentiated on Braided Polylactide Scaffolds Is a Potential Approach for Tendon Tissue Engineering, Tissue Eng.Part A., Vol. 22, No. 5-6, 2016, pp. 513-523.

[108] H. Deplaine, M. Lebourg, P. Ripalda, A. Vidaurre, P. Sanz-Ramos, G. Mora, F. Prosper, I. Ochoa, M. Doblare, J.L. Gomez Ribelles, I. Izal-Azcarate, G. Gallego Ferrer, Biomimetic hydroxyapatite coating on pore walls improves osteointegration of poly(L-lactic acid) scaffolds, J.Biomed.Mater.Res.B.Appl.Biomater., Vol. 101, No. 1, 2013, pp. 173-186.

[109] M. Huttunen, Analysis of the factors affecting the inherent viscosity of oriented polylactides during hydrolytic degradation, J.Mater.Sci.Mater.Med., Vol. 24, No. 5, 2013, pp. 1131-1144.

[110] M. Kellomaki, H. Niiranen, K. Puumanen, N. Ashammakhi, T. Waris, P. Tormala, Bioabsorbable scaffolds for guided bone regeneration and generation, Biomaterials, Vol. 21, No. 24, 2000, pp. 2495-2505.

[111] S.H. Kim, Y. Jung, S.H. Kim, A biocompatible tissue scaffold produced by supercritical fluid processing for cartilage tissue engineering, Tissue Eng.Part C.Methods, Vol. 19, No. 3, 2013, pp. 181-188.

[112] J. Yao, S.L. Tao, M.J. Young, Synthetic Polymer Scaffolds for Stem Cell Transplantation in Retinal Tissue Engineering, Polymers (20734360), Vol. 3, No. 2, 2011, pp. 899-914.

[113] M.A. Woodruff & D.W. Hutmacher, The return of a forgotten polymer—Polycaprolactone in the 21st century, Progress in Polymer Science, Vol. 35, No. 10, 2010, pp. 1217-1256.

[114] A.B. Yeatts, S.K. Both, W. Yang, H.S. Alghamdi, F. Yang, J.P. Fisher, J.A. Jansen, In vivo bone regeneration using tubular perfusion system bioreactor cultured nanofibrous scaffolds, Tissue Eng.Part A., Vol. 20, No. 1-2, 2014, pp. 139-146.

[115] R. Sartoneva, A.M. Haaparanta, T. Lahdes-Vasama, B. Mannerstrom, M. Kellomaki, M. Salomaki, G. Sandor, R. Seppanen, S. Miettinen, S. Haimi, Characterizing and optimizing poly-L-lactide-co-epsilon-caprolactone membranes for urothelial tissue engineering, J.R.Soc.Interface, Vol. 9, No. 77, 2012, pp. 3444-3454.

[116] R. Sartoneva, S. Haimi, S. Miettinen, B. Mannerstrom, A.M. Haaparanta, G.K. Sandor, M. Kellomaki, R. Suuronen, T. Lahdes-Vasama, Comparison of a poly-L-lactide-co-epsilon-caprolactone and human amniotic membrane for urothelium tissue engineering applications, J.R.Soc.Interface, Vol. 8, No. 58, 2011, pp. 671-677.

[117] P. Habibovic, M.C. Kruyt, M.V. Juhl, S. Clyens, R. Martinetti, L. Dolcini, N. Theilgaard, C.A. van Blitterswijk, Comparative in vivo study of six hydroxyapatite-based bone graft substitutes, J.Orthop.Res., Vol. 26, No. 10, 2008, pp. 1363-1370.

[118] G. Hannink & J.J. Arts, Bioresorbability, porosity and mechanical strength of bone substitutes: what is optimal for bone regeneration? Injury, Vol. 42 Suppl 2, 2011, pp. S22-5.

[119] S.I. Roohani-Esfahani, C.R. Dunstan, J.J. Li, Z. Lu, B. Davies, S. Pearce, J. Field, R. Williams, H. Zreiqat, Unique microstructural design of ceramic scaffolds for bone regeneration under load, Acta Biomater., Vol. 9, No. 6, 2013, pp. 7014-7024.

[120] D.A. Gaspar, V. Gomide, F.J. Monteiro, The role of perfusion bioreactors in bone tissue engineering, Biomatter, Vol. 2, No. 4, 2012, pp. 167-175.

[121] R. Yunus Basha, T.S. Sampath Kumar, M. Doble, Design of biocomposite materials for bone tissue regeneration, Mater.Sci.Eng.C.Mater.Biol.Appl., Vol. 57, 2015, pp. 452-463.

[122] K. Rezwan, Q.Z. Chen, J.J. Blaker, A.R. Boccaccini, Biodegradable and bioactive porous polymer/inorganic composite scaffolds for bone tissue engineering, Biomaterials, Vol. 27, No. 18, 2006, pp. 3413-3431.

[123] P. Kasten, I. Beyen, P. Niemeyer, R. Luginbuhl, M. Bohner, W. Richter, Porosity and pore size of beta-tricalcium phosphate scaffold can influence protein production and osteogenic differentiation of human mesenchymal stem cells: an in vitro and in vivo study, Acta Biomater., Vol. 4, No. 6, 2008, pp. 1904-1915.

[124] L.S. Gardel, L.A. Serra, R.L. Reis, M.E. Gomes, Use of perfusion bioreactors and large animal models for long bone tissue engineering, Tissue Eng.Part B.Rev., Vol. 20, No. 2, 2014, pp. 126-146.

[125] K.C. Hicok, T.V. Du Laney, Y.S. Zhou, Y.D. Halvorsen, D.C. Hitt, L.F. Cooper, J.M. Gimble, Human adipose-derived adult stem cells produce osteoid in vivo, Tissue Eng., Vol. 10, No. 3-4, 2004, pp. 371-380.

[126] R.Z. Birk, L. Abramovitch-Gottlib, I. Margalit, M. Aviv, E. Forti, S. Geresh, R. Vago, Conversion of adipogenic to osteogenic phenotype using crystalline porous biomatrices of marine origin, Tissue Eng., Vol. 12, No. 1, 2006, pp. 21-31.

[127] G. Bouet, D. Marchat, M. Cruel, L. Malaval, L. Vico, In vitro three-dimensional bone tissue models: from cells to controlled and dynamic environment, Tissue Eng.Part B.Rev., Vol. 21, No. 1, 2015, pp. 133-156.

[128] M. Bhamidipati, A.M. Scurto, M.S. Detamore, The future of carbon dioxide for polymer processing in tissue engineering, Tissue Eng.Part B.Rev., Vol. 19, No. 3, 2013, pp. 221-232.

[129] A. Zhang, Q. Zhang, H. Bai, L. Li, J. Li, Polymeric nanoporous materials fabricated with supercritical CO2 and CO2-expanded liquids, Chem.Soc.Rev., Vol. 43, No. 20, 2014, pp. 6938-6953.

[130] G.A. Villalona, B. Udelsman, D.R. Duncan, E. McGillicuddy, R.F. Sawh-Martinez, N. Hibino, C. Painter, T. Mirensky, B. Erickson, T. Shinoka, C.K. Breuer, Cell-seeding techniques in vascular tissue engineering, Tissue Eng.Part B.Rev., Vol. 16, No. 3, 2010, pp. 341-350.

[131] S. Concaro, E. Nicklasson, L. Ellowsson, A. Lindahl, M. Brittberg, P. Gatenholm, Effect of cell seeding concentration on the quality of tissue engineered constructs loaded with adult human articular chondrocytes, J.Tissue Eng.Regen.Med., Vol. 2, No. 1, 2008, pp. 14-21.

[132] N.A. Plunkett, S. Partap, F.J. O'Brien, Osteoblast response to rest periods during bioreactor culture of collagen-glycosaminoglycan scaffolds, Tissue Eng.Part A., Vol. 16, No. 3, 2010, pp. 943-951.

[133] S.L. Ishaug, G.M. Crane, M.J. Miller, A.W. Yasko, M.J. Yaszemski, A.G. Mikos, Bone formation by three-dimensional stromal osteoblast culture in biodegradable polymer scaffolds, J.Biomed.Mater.Res., Vol. 36, No. 1, 1997, pp. 17-28.

[134] J.C. Bodle, A.D. Hanson, E.G. Loboa, Adipose-derived stem cells in functional bone tissue engineering: lessons from bone mechanobiology, Tissue Eng.Part B.Rev., Vol. 17, No. 3, 2011, pp. 195-211.

[135] F.W. Janssen, J. Oostra, A. Oorschot, C.A. van Blitterswijk, A perfusion bioreactor system capable of producing clinically relevant volumes of tissue-engineered bone: in vivo bone formation showing proof of concept, Biomaterials, Vol. 27, No. 3, 2006, pp. 315-323.

[136] D.A. Gaspar, V. Gomide, F.J. Monteiro, The role of perfusion bioreactors in bone tissue engineering, Biomatter, Vol. 2, No. 4, 2012, pp. 167-175.

[137] A.B. Yeatts & J.P. Fisher, Bone tissue engineering bioreactors: dynamic culture and the influence of shear stress, Bone, Vol. 48, No. 2, 2011, pp. 171-181.

[138] A.B. Yeatts, D.T. Choquette, J.P. Fisher, Bioreactors to influence stem cell fate: augmentation of mesenchymal stem cell signaling pathways via dynamic culture systems, Biochim.Biophys.Acta, Vol. 1830, No. 2, 2013, pp. 2470-2480.

[139] A.J. Salgado, M.E. Gomes, R.L. Reis, Tissue Engineering of Mineralized Tissues, Proceedings of the NATO Advanced Study Institute, Alvor, Algarve, Portugal, 13–24 October 2003, NATO Science Series II: Mathematics, Physics and Chemistry, Vol. 171, 2005, pp. 205-222.

[140] L.E. Freed & G. Vunjak-Novakovic, Tissue engineering bioreactors, Academic Press, San Diego, CA, USA, 2000, pp. 143-156.

[141] V.I. Sikavitsas, G.N. Bancroft, A.G. Mikos, Formation of three-dimensional cell/polymer constructs for bone tissue engineering in a spinner flask and a rotating wall vessel bioreactor, J.Biomed.Mater.Res., Vol. 62, No. 1, 2002, pp. 136-148.

[142] A.S. Goldstein, T.M. Juarez, C.D. Helmke, M.C. Gustin, A.G. Mikos, Effect of convection on osteoblastic cell growth and function in biodegradable polymer foam scaffolds, Biomaterials, Vol. 22, No. 11, 2001, pp. 1279-1288.

[143] J.M. García-Aznar, P. Moreo, V. Alastrué, V. Acosta, I. Ochoa, J. Peña, V. Cabañas, J. Román, M. Vallet-RegíM. Doblaré. A new continuous perfusion bioreactor system for tissue growth and scaffold permeability measurement. 2 nd TERMIS World Meeting, Seoul, South Korea, August 31 - September 3, 2009.

[144] H.L. Holtorf, J.A. Jansen, A.G. Mikos, Modulation of cell differentiation in bone tissue engineering constructs cultured in a bioreactor, Adv.Exp.Med.Biol., Vol. 585, 2006, pp. 225-241.

[145] H.L. Holtorf, T.L. Sheffield, C.G. Ambrose, J.A. Jansen, A.G. Mikos, Flow perfusion culture of marrow stromal cells seeded on porous biphasic calcium phosphate ceramics, Ann.Biomed.Eng., Vol. 33, No. 9, 2005, pp. 1238-1248.

[146] B.D. Porter, A.S. Lin, A. Peister, D. Hutmacher, R.E. Guldberg, Noninvasive image analysis of 3D construct mineralization in a perfusion bioreactor, Biomaterials, Vol. 28, No. 15, 2007, pp. 2525-2533.

[147] H.L. Holtorf, J.A. Jansen, A.G. Mikos, Flow perfusion culture induces the osteoblastic differentiation of marrow stroma cell-scaffold constructs in the absence of dexamethasone, J.Biomed.Mater.Res.A., Vol. 72, No. 3, 2005, pp. 326-334.

[148] M.R. Kreke, L.A. Sharp, Y.W. Lee, A.S. Goldstein, Effect of intermittent shear stress on mechanotransductive signaling and osteoblastic differentiation of bone marrow stromal cells, Tissue Eng.Part A., Vol. 14, No. 4, 2008, pp. 529-537.

[149] J. Klein-Nulend, E.H. Burger, C.M. Semeins, L.G. Raisz, C.C. Pilbeam, Pulsating fluid flow stimulates prostaglandin release and inducible prostaglandin G/H synthase mRNA expression in primary mouse bone cells, J.Bone Miner.Res., Vol. 12, No. 1, 1997, pp. 45-51.

[150] N.N. Batra, Y.J. Li, C.E. Yellowley, L. You, A.M. Malone, C.H. Kim, C.R. Jacobs, Effects of short-term recovery periods on fluid-induced signaling in osteoblastic cells, J.Biomech., Vol. 38, No. 9, 2005, pp. 1909-1917.

[151] S.H. Cartmell, B.D. Porter, A.J. Garcia, R.E. Guldberg, Effects of medium perfusion rate on cell-seeded three-dimensional bone constructs in vitro, Tissue Eng., Vol. 9, No. 6, 2003, pp. 1197-1203.

[152] M.R. Kreke, W.R. Huckle, A.S. Goldstein, Fluid flow stimulates expression of osteopontin and bone sialoprotein by bone marrow stromal cells in a temporally dependent manner, Bone, Vol. 36, No. 6, 2005, pp. 1047-1055.

[153] Y.J. Li, N.N. Batra, L. You, S.C. Meier, I.A. Coe, C.E. Yellowley, C.R. Jacobs, Oscillatory fluid flow affects human marrow stromal cell proliferation and differentiation, J.Orthop.Res., Vol. 22, No. 6, 2004, pp. 1283-1289.

[154] K.M. Reich & J.A. Frangos, Effect of flow on prostaglandin E2 and inositol trisphosphate levels in osteoblasts, Am.J.Physiol., Vol. 261, No. 3 Pt 1, 1991, pp. C428-32.

[155] J. You, G.C. Reilly, X. Zhen, C.E. Yellowley, Q. Chen, H.J. Donahue, C.R. Jacobs, Osteopontin gene regulation by oscillatory fluid flow via intracellular calcium mobilization and activation of mitogen-activated protein kinase in MC3T3-E1 osteoblasts, J.Biol.Chem., Vol. 276, No. 16, 2001, pp. 13365-13371.

[156] Z.Y. Zhang, S.H. Teoh, J.H. Hui, N.M. Fisk, M. Choolani, J.K. Chan, The potential of human fetal mesenchymal stem cells for off-the-shelf bone tissue engineering application, Biomaterials, Vol. 33, No. 9, 2012, pp. 2656-2672.

[157] M. Frohlich, W.L. Grayson, D. Marolt, J.M. Gimble, N. Kregar-Velikonja, G. Vunjak-Novakovic, Bone grafts engineered from human adipose-derived stem cells in perfusion bioreactor culture, Tissue Eng.Part A., Vol. 16, No. 1, 2010, pp. 179-189.

[158] W. Baumgartner, M. Welti, N. Hild, S.C. Hess, W.J. Stark, G.M. Burgisser, P. Giovanoli, J. Buschmann, Tissue mechanics of piled critical size biomimetic and biominerizable nanocomposites: Formation of bioreactor-induced stem cell gradients under perfusion and compression, J.Mech.Behav.Biomed.Mater., Vol. 47, 2015, pp. 124-134.

[159] S. Guven, A. Mehrkens, F. Saxer, D.J. Schaefer, R. Martinetti, I. Martin, A. Scherberich, Engineering of large osteogenic grafts with rapid engraftment capacity using mesenchymal and endothelial progenitors from human adipose tissue, Biomaterials, Vol. 32, No. 25, 2011, pp. 5801-5809.

[160] A. Scherberich, R. Galli, C. Jaquiery, J. Farhadi, I. Martin, Three-dimensional perfusion culture of human adipose tissue-derived endothelial and osteoblastic progenitors generates osteogenic constructs with intrinsic vascularization capacity, Stem Cells, Vol. 25, No. 7, 2007, pp. 1823-1829.

[161] D. Li, T. Tang, J. Lu, K. Dai, Effects of flow shear stress and mass transport on the construction of a large-scale tissue-engineered bone in a perfusion bioreactor, Tissue Eng.Part A., Vol. 15, No. 10, 2009, pp. 2773-2783.

[162] F. Zhao, R. Chella, T. Ma, Effects of shear stress on 3-D human mesenchymal stem cell construct development in a perfusion bioreactor system: Experiments and hydrodynamic modeling, Biotechnol.Bioeng., Vol. 96, No. 3, 2007, pp. 584-595.

[163] C. Kleinhans, R.R. Mohan, G. Vacun, T. Schwarz, B. Haller, Y. Sun, A. Kahlig, P. Kluger, A. Finne-Wistrand, H. Walles, J. Hansmann, A perfusion bioreactor system efficiently generates cell-loaded bone substitute materials for addressing critical size bone defects, Biotechnol.J., Vol. 10, No. 11, 2015, pp. 1727-1738.

[164] G.N. Bancroft, V.I. Sikavitsas, J. van den Dolder, T.L. Sheffield, C.G. Ambrose, J.A. Jansen, A.G. Mikos, Fluid flow increases mineralized matrix deposition in 3D perfusion culture of marrow stromal osteoblasts in a dose-dependent manner, Proc.Natl.Acad.Sci.U.S.A., Vol. 99, No. 20, 2002, pp. 12600-12605.

[165] R.A. Thibault, A.G. Mikos, F.K. Kasper, Protein and mineral composition of osteogenic extracellular matrix constructs generated with a flow perfusion bioreactor, Biomacromolecules, Vol. 12, No. 12, 2011, pp. 4204-4212.

[166] M. Bartnikowski, T.J. Klein, F.P. Melchels, M.A. Woodruff, Effects of scaffold architecture on mechanical characteristics and osteoblast response to static and perfusion bioreactor cultures, Biotechnol.Bioeng., Vol. 111, No. 7, 2014, pp. 1440-1451.

[167] W.L. Grayson, S. Bhumiratana, C. Cannizzaro, P.H. Chao, D.P. Lennon, A.I. Caplan, G. Vunjak-Novakovic, Effects of initial seeding density and fluid perfusion rate on formation of tissue-engineered bone, Tissue Eng.Part A., Vol. 14, No. 11, 2008, pp. 1809-1820.

[168] F.W. Janssen, J. Oostra, A. Oorschot, C.A. van Blitterswijk, A perfusion bioreactor system capable of producing clinically relevant volumes of tissue-engineered bone: in vivo bone formation showing proof of concept, Biomaterials, Vol. 27, No. 3, 2006, pp. 315-323.

[169] TA Instruments. 2016, TA Instruments 3D CulturePro™ Bioreactors. [WWW]. Available, (accessed 15.08.2016): http://www.tainstruments.com/3dculturepro-bioreactors/.

[170] EBERS Medical. 2016, Automated dynamic cell seeding of ceramic scaffolds for tissue engineering. [WWW]. Available, (accessed 15.08.2016): http://www.ebersmedical.com/files/technical_notes/CellSeeding_TN.pdf.

[171] L.G. Cox, B. van Rietbergen, C.C. van Donkelaar, K. Ito, Analysis of bone architecture sensitivity for changes in mechanical loading, cellular activity, mechanotransduction, and tissue properties, Biomech.Model.Mechanobiol, Vol. 10, No. 5, 2011, pp. 701-712.

[172] K. Paakinaho, H. Heino, J. Vaisanen, P. Tormala, M. Kellomaki, Effects of lactide monomer on the hydrolytic degradation of poly(lactide-co-glycolide) 85L/15G, J.Mech.Behav.Biomed.Mater., Vol. 4, No. 7, 2011, pp. 1283-1290.

[173] P.A. Zuk, M. Zhu, P. Ashjian, D.A. De Ugarte, J.I. Huang, H. Mizuno, Z.C. Alfonso, J.K. Fraser, P. Benhaim, M.H. Hedrick, Human adipose tissue is a source of multipotent stem cells, Mol.Biol.Cell, Vol. 13, No. 12, 2002, pp. 4279-4295.

[174] T. Rada, R.L. Reis, M.E. Gomes, Adipose tissue-derived stem cells and their application in bone and cartilage tissue engineering, Tissue Eng.Part B.Rev., Vol. 15, No. 2, 2009, pp. 113-125.

[175] M.J. Jaroszeski & G. Radcliff, Fundamentals of flow cytometry, Mol.Biotechnol., Vol. 11, No. 1, 1999, pp. 37-53.

[176] K. McIntosh, S. Zvonic, S. Garrett, J.B. Mitchell, Z.E. Floyd, L. Hammill, A. Kloster, Y. Di Halvorsen, J.P. Ting, R.W. Storms, B. Goh, G. Kilroy, X. Wu, J.M. Gimble, The immunogenicity of human adipose-derived cells: temporal changes in vitro, Stem Cells, Vol. 24, No. 5, 2006, pp. 1246-1253.

[177] H. Tapp, E.N. Hanley Jr, J.C. Patt, H.E. Gruber, Adipose-derived stem cells: characterization and current application in orthopaedic tissue repair, Exp.Biol.Med.(Maywood), Vol. 234, No. 1, 2009, pp. 1-9.

[178] S. Haimi, L. Moimas, E. Pirhonen, B. Lindroos, H. Huhtala, S. Raty, H. Kuokkanen, G.K. Sandor, S. Miettinen, R. Suuronen, Calcium phosphate surface treatment of bioactive glass causes a delay in early osteogenic differentiation of adipose stem cells, J.Biomed.Mater.Res.A., Vol. 91, No. 2, 2009, pp. 540-547.

[179] R.G. Bacabac, D. Mizuno, C.F. Schmidt, F.C. MacKintosh, J.J. Van Loon, J. Klein-Nulend, T.H. Smit, Round versus flat: bone cell morphology, elasticity, and mechanosensing, J.Biomech., Vol. 41, No. 7, 2008, pp. 1590-1598.

[180] S.H. Cartmell, B.D. Porter, A.J. Garcia, R.E. Guldberg, Effects of medium perfusion rate on cell-seeded three-dimensional bone constructs in vitro, Tissue Eng., Vol. 9, No. 6, 2003, pp. 1197-1203.

[181] T. Mygind, M. Stiehler, A. Baatrup, H. Li, X. Zou, A. Flyvbjerg, M. Kassem, C. Bunger, Mesenchymal stem cell ingrowth and differentiation on coralline hydroxyapatite scaffolds, Biomaterials, Vol. 28, No. 6, 2007, pp. 1036-1047.

[182] M. Shin, H. Yoshimoto, J.P. Vacanti, In vivo bone tissue engineering using mesenchymal stem cells on a novel electrospun nanofibrous scaffold, Tissue Eng., Vol. 10, No. 1-2, 2004, pp. 33-41.

[183] L. Kyllonen, S. Haimi, J. Sakkinen, H. Kuokkanen, B. Mannerstrom, G.K. Sandor, S. Miettinen, Exogenously added BMP-6, BMP-7 and VEGF may not enhance the osteogenic differentiation of human adipose stem cells, Growth Factors, Vol. 31, No. 5, 2013, pp. 141-153.

[184] M. Ojansivu, S. Vanhatupa, L. Bjorkvik, H. Hakkanen, M. Kellomaki, R. Autio, J.A. Ihalainen, L. Hupa, S. Miettinen, Bioactive glass ions as strong enhancers of osteogenic differentiation in human adipose stem cells, Acta Biomater., Vol. 21, 2015, pp. 190-203.

[185] Y. Wang, T. Uemura, J. Dong, H. Kojima, J. Tanaka, T. Tateishi, Application of perfusion culture system improves in vitro and in vivo osteogenesis of bone marrow-derived osteoblastic cells in porous ceramic materials, Tissue Eng., Vol. 9, No. 6, 2003, pp. 1205-1214.

[186] A.R. Silva, A.C. Paula, T.M. Martins, A.M. Goes, M.M. Pereria, Synergistic effect between bioactive glass foam and a perfusion bioreactor on osteogenic differentiation of human adipose stem cells, J.Biomed.Mater.Res.A., Vol. 102, No. 3, 2014, pp. 818-827.

[187] T. Okabe, M. Sakamoto, H. Takeuchi, K. Matsushima, Effects of pH on mineralization ability of human dental pulp cells, J.Endod., Vol. 32, No. 3, 2006, pp. 198-201.

[188] K. Kim, A. Yeatts, D. Dean, J.P. Fisher, Stereolithographic bone scaffold design parameters: osteogenic differentiation and signal expression, Tissue Eng.Part B.Rev., Vol. 16, No. 5, 2010, pp. 523-539.

[189] V.A. Acosta Santamaria, M. Malve, A. Duizabo, A. Mena Tobar, G. Gallego Ferrer, J.M. Garcia Aznar, M. Doblare, I. Ochoa, Computational methodology to determine fluid related parameters of non regular three-dimensional scaffolds, Ann.Biomed.Eng., Vol. 41, No. 11, 2013, pp. 2367-2380.

[190] A. Ronca, L. Ambrosio, D.W. Grijpma, Preparation of designed poly(d,l-lactide)/nanosized hydroxyapatite composite structures by stereolithography, Acta Biomater., Vol. 9, No. 4, 2013, pp. 5989-96.

[191] S. Truscello, G. Kerckhofs, S. Van Bael, G. Pyka, J. Schrooten, H. Van Oosterwyck, Prediction of permeability of regular scaffolds for skeletal tissue engineering: a combined computational and experimental study, Acta Biomater., Vol. 8, No. 4, 2012, pp. 1648-1658.

[192] M.R. Dias, P.R. Fernandes, J.M. Guedes, S.J. Hollister, Permeability analysis of scaffolds for bone tissue engineering, J.Biomech., Vol. 45, No. 6, 2012, pp. 938-944.

[193] J. Pan, T. Zhang, L. Mi, B. Zhang, B. Wang, L. Yang, L. Deng, L. Wang, Stepwise increasing and decreasing fluid shear stresses differentially regulate the functions of osteoblasts, Cell.Mol.Bioeng., Vol. 3, No. 4, 2010, pp. 376-386.

[194] W.L. Grayson, S. Bhumiratana, P.H. Grace Chao, C.T. Hung, G. Vunjak-Novakovic, Spatial regulation of human mesenchymal stem cell differentiation in engineered osteochondral constructs: effects of pre-differentiation, soluble factors and medium perfusion, Osteoarthritis Cartilage, Vol. 18, No. 5, 2010, pp. 714-723.

[195] K.D. Kavlock & A.S. Goldstein, Effect of pulse frequency on the osteogenic differentiation of mesenchymal stem cells in a pulsatile perfusion bioreactor, J.Biomech.Eng., Vol. 133, No. 9, 2011, pp. 091005.

[196] J. Filipowska, G.C. Reilly, A.M. Osyczka, A single short session of media perfusion induces osteogenesis in hBMSCs cultured in porous scaffolds, dependent on cell differentiation stage, Biotechnol.Bioeng., Vol. 113, No. 8, 2016, pp. 1814-24.

[197] N. Bolgen, Y. Yang, P. Korkusuz, E. Guzel, A.J. El Haj, E. Piskin, Three-dimensional ingrowth of bone cells within biodegradable cryogel scaffolds in bioreactors at different regimes, Tissue Eng.Part A., Vol. 14, No. 10, 2008, pp. 1743-1750.

[198] M.R. Kreke, L.A. Sharp, Y.W. Lee, A.S. Goldstein, Effect of intermittent shear stress on mechanotransductive signaling and osteoblastic differentiation of bone marrow stromal cells, Tissue Eng.Part A., Vol. 14, No. 4, 2008, pp. 529-537.

[199] A.G. Robling, D.B. Burr, C.H. Turner, Recovery periods restore mechanosensitivity to dynamically loaded bone, J.Exp.Biol., Vol. 204, No. Pt 19, 2001, pp. 3389-3399.

[200] K.D. Kavlock & A.S. Goldstein, Effect of pulse frequency on the osteogenic differentiation of mesenchymal stem cells in a pulsatile perfusion bioreactor, J.Biomech.Eng., Vol. 133, No. 9, 2011, pp. 091005.

[201] L.A. Sharp, Y.W. Lee, A.S. Goldstein, Effect of low-frequency pulsatile flow on expression of osteoblastic genes by bone marrow stromal cells, Ann.Biomed.Eng., Vol. 37, No. 3, 2009, pp. 445-453.

[202] M. Bjorninen, A. Siljander, J. Pelto, J. Hyttinen, M. Kellomaki, S. Miettinen, R. Seppanen, S. Haimi, Comparison of chondroitin sulfate and hyaluronic Acid doped conductive polypyrrole films for adipose stem cells, Ann.Biomed.Eng., Vol. 42, No. 9, 2014, pp. 1889-1900.

[203] M.D. Zhao, M. Bjorninen, L. Cao, H.R. Wang, J. Pelto, X.Q. Li, J. Hyttinen, Y.Q. Jiang, M. Kellomaki, S. Miettinen, G.K. Sandor, R. Seppanen, S. Haimi, J. Dong, Polypyrrole coating on poly-(lactide/glycolide)-beta-tricalcium phosphate screws enhances new bone formation in rabbits, Biomed.Mater., Vol. 10, No. 6, 2015, pp. 065016-6041/10/6/065016.

[204] S. Weinbaum, S.C. Cowin, Y. Zeng, A model for the excitation of osteocytes by mechanical loading-induced bone fluid shear stresses, J.Biomech., Vol. 27, No. 3, 1994, pp. 339-360.

[205] G. Uzer, S.L. Manske, M.E. Chan, F.P. Chiang, C.T. Rubin, M.D. Frame, S. Judex, Separating Fluid Shear Stress from Acceleration during Vibrations in Vitro: Identification of Mechanical Signals Modulating the Cellular Response, Cell.Mol.Bioeng., Vol. 5, No. 3, 2012, pp. 266-276.

[206] Y. Guyot, F.P. Luyten, J. Schrooten, I. Papantoniou, L. Geris, A three-dimensional computational fluid dynamics model of shear stress distribution during neotissue growth in a perfusion bioreactor, Biotechnol.Bioeng., Vol. 112, No. 12, 2015, pp. 2591-2600.

[207] L. Ferroni, I. Tocco, A. De Pieri, M. Menarin, E. Fermi, A. Piattelli, C. Gardin, B. Zavan, Pulsed magnetic therapy increases osteogenic differentiation of mesenchymal stem cells only if they are pre-committed, Life Sci., Vol. 152, 2016, pp. 44-51.

[208] H.M. Du, X.H. Zheng, L.Y. Wang, W. Tang, L. Liu, W. Jing, Y.F. Lin, W.D. Tian, J. Long, The osteogenic response of undifferentiated human adipose-derived stem cells under mechanical stimulation, Cells Tissues Organs, Vol. 196, No. 4, 2012, pp. 313-324.

[209] D. Prè, G. Ceccarelli, Cusella De Angelis, M. G.G. Magenes, High frequency mechanical vibrations stimulate the bone matrix formation in hBMSCs. XII Mediterranean Conference on Medical and Biological Engineering and Computing, 2010, Vol. 29, IFMBE Proceedings, pp. 494-497.

[210] M. Ding, S.S. Henriksen, D. Wendt, S. Overgaard, An automated perfusion bioreactor for the streamlined production of engineered osteogenic grafts, J.Biomed.Mater.Res.B.Appl.Biomater., Vol. 104, No. 3, 2016, pp. 532-537.